Sum-Frequency Generation at interfaces: a Fresnel story I. Designing high contrast in two interface systems

Bertrand Busson

Sum-Frequency Generation at interfaces: a Fresnel story

I. Designing high contrast in two interface systems

Bertrand Busson

Université Paris-Saclay, CNRS, Institut de Chimie Physique, UMR 8000, 91405 ORSAY, France[a)]

(Dated: 1 June 2023)

When a homogeneous film of finite thickness is optically probed, interference due to multiple reflections modulates in amplitude the electric field of light. For optical processes located only at the interfaces between two media, as is common for Sum-Frequency Generation (SFG), interference also modulates the contrast between signals generated at the entrance and exit planes of the film. We introduce a universal formalism for the Fresnel factors, which bear all the information about interference, valid at any point in a three-layer system and for the three beams involved in the SFG process. Their analysis provides general rules for obtaining a high contrast. In particular, we define four configurations leading to the cancellation of the SFG response from the entrance side of the film when its thickness or the angles of incidence are tuned. Cancellation conditions depend on the polarization of light and follow simple analytical rules, leading to a straightforward experimental implementation. Such a selective cancellation makes it possible to independently measure single components of the nonlinear susceptibility, for example in a ppp experiment, and to separate surface from bulk response, by combining a few measurements.

[a)]Electronic mail: bertrand.busson@universite-paris-saclay.fr

I. INTRODUCTION

Second-order nonlinear optical tools, among which Sum-Frequency Generation (SFG) spectroscopy plays a leading role, are by essence sensitive to interfaces because of their symmetry properties: processes at the electric dipole level (i.e. their leading order) vanish in a centrosymmetric bulk but contribute to measurable signals at the interface between two such bulks, where the symmetry is locally broken. This sensitivity has been demonstrated in solid, liquid, gaseous and vacuum environments, at organic and mineral interfaces, and extensively applied to heterogeneous catalysis,[1] electrocatalysis,[2] and reactivity at water interfaces,[3] to name a few. Most examples deal with monolayers or ultrathin layers, for which SFG has become a specialized tool.[4] However, some other studies focus on thicker films, for fundamental purposes[5] or driven by applications.[6] As recalled in Ref. 7, "all films thicker than a monolayer have two interfaces". This introduces a fundamental difference between ultrathin and thick films, as they possess in principle one and two sources for SFG signals, respectively. For the thick films, interference between both sources is an essential parameter to take into account, generating new effects as a function of the film thickness and angles of incidence.[5]

The basic equation governing all second order nonlinear processes at the dipolar level, relating the electric fields of the sources to the nonlinear polarization, is very simple and does not depend at all on the nature or structure of the probed material, nor on experimental geometry. A dedicated formalism has been elaborated to transform in a second step this equation into formulas relating the measurable quantities, i.e. intensities of emitted light and of incoming beams, in the bulk[8] and at plane homogeneous interfaces.[9,10] At this stage, it must be accounted for that the nonlinear process actually happens in a medium or at an interface belonging to a system comprising several media. This is properly done by introducting the effective nonlinear surface susceptibility and the associated Fresnel factors, which are thus specific of the definition of the whole system and of the experimental geometries. For example, they differ between reflected and transmitted geometries, and depend in which medium or at which interface the nonlinear process is supposed to happen. In practice, for a system involving up to three media, "monolayer" people pick up their factors among a few models: two-layer, three-layer or L/K model, as detailed below. For thicker layers, a consensus has arisen to a common "thin film" formalism[11–13], defining distinct Fres-

nel factors for the first and second interface, whereas alternate formulations exist,[14] e.g. the Abelès[15] and transfer matrix[16,17] formalisms. These will be discussed in details in the next paper[18] but have been shown to lead to the same results as the thin film model in the three layer case.[15] The thin film model of the literature has some limitations: Fresnel factors for emitted and incident beams differ as for their phases, the link between factors evaluated at the first and second interface does not appear straightforward (the alternate formalisms may solve some of these issues), and there is no generic formula for a nonlinear process happening at neither of the two interfaces but at arbitrary depth somewhere in between (even if some attempts exist[19]).

Considering the existence of two interfaces in a thick film, generating SFG light beams which eventually interfere to produce the experimental signals, one may wonder whether it is possible to suppress one of these emitted beams and probe only the other interface, in other words tune the experimental contrast between both interfaces towards extreme values. In this way, one would be able to build systems with two interfaces, thus two SFG sources, while probing only one and making the other silent. From the models above, this has been shown possible using various experimental configurations and systems.[15,20–24] The underlying reasons are sometimes difficult to understand, even if it is known that they are due to the interference process in the film.

In this article, we first review the essential, but necessary, features and properties of Fresnel factors in systems with one and two interfaces. These steps allow to understand on which grounds the various models found in the literature differ; why the Fresnel factors for the reflected SFG beam are necessary equal to those of the incoming beams; how these factors in a thin film model may be universally defined for an arbitrary depth inside the film, including both interfaces, using a single set of equations; and why they encompass all alone the complexity of the interface (number of interfaces, thicknesses, interference) wherever the nonlinear process is considered, while the definitions of emitted intensities and effective nonlinear susceptibility don't change. Rules for enhanced contrast in the thin film model are then established in the general case from the relative values of Fresnel factors at the first and second interface. In particular, we show that it is possible to minimize and even cancel the SFG response from the first interface in four distinct configurations by adjusting the angles of incidence and the film thickness, the latter taking periodic or single values depending on the phenomenon giving birth to the minimum (i.e. propagation or absorption). We also

illustrate how specific choices of the experimental parameters lead to cancellation (or to a minimum) for several components of the effective hyperpolarizability at the same time.

II. SYSTEMS WITH ONE INTERFACE

A. Foreword about conventions

In the following, we treat the Sum-Frequency Generation (SFG) process, i.e. nonlinear three-wave mixing, at an interface defined as a succession of parallel planes of homogeneous and isotropic material, all beams being supposed to travel in a common plane of incidence. In the literature, the conventions for the definitions of ($\boldsymbol{s}$,$\boldsymbol{p}$) polarization vectors and the laboratory ($\boldsymbol{x}$,$\boldsymbol{y}$,$\boldsymbol{z}$) frame attached to the interface may vary. Following the usual choice, plane of incidence is defined as ($\boldsymbol{x}$,$\boldsymbol{z}$). The orientation of $\boldsymbol{z}$ axis is perpendicular to the interface, but its direction usually points "up" [i.e. towards the incoming light beams, see Fig. 1(A)] for SFG produced in a reflection geometry for simple systems composed of one or two interfaces;[5,12,25,26] and "down" (i.e. towards the forward direction of beam propagation) for multilayer systems[15,27] or when bulk contributions are considered,[28,29] with exceptions in either case.[8,10,17,30] This has consequences on the signs of the propagation phases along $\boldsymbol{z}$ (from Part. III onwards) and of the mutual projections of unit vectors between bases ($\boldsymbol{s}$,$\boldsymbol{p}$) and ($\boldsymbol{x}$,$\boldsymbol{y}$,$\boldsymbol{z}$). Reversing the orientation of $\boldsymbol{z}$ axis also changes the signs of the nonlinear susceptibility components involving an odd number of z terms, i.e. all components when the interface is isotropic, this sign ambiguity being resolved when molecular hyperpolarizability components are introduced and projected onto the laboratory frame.[31,32] In order to adopt a common convention for the whole article, we define [Fig. 1(A)] the $\boldsymbol{z}$ vector pointing "up", all $\boldsymbol{p}$ vectors having a positive component along $\boldsymbol{z}$, with a positive (resp. negative) x-component for the incoming (resp. reflected) $\boldsymbol{p}$ vectors in co-propagating geometry. This fixes the sign of the reflection coefficient r_p for p polarized light (see Eq. 5 below, while opposite conventions exist[17]). Finally, using $\boldsymbol{s} = \boldsymbol{n} \times \boldsymbol{p}$ where $\boldsymbol{n}$ is the unit wavevector, we find $\boldsymbol{s} = -\boldsymbol{y}$ for the transverse polarization, which is not a universal convention either. As long as a constant choice for either y or s as the transverse coordinate is assumed, this has no influence on the results.

As for notations, we index quantities (refractive indices n, angles of incidence θ, electric

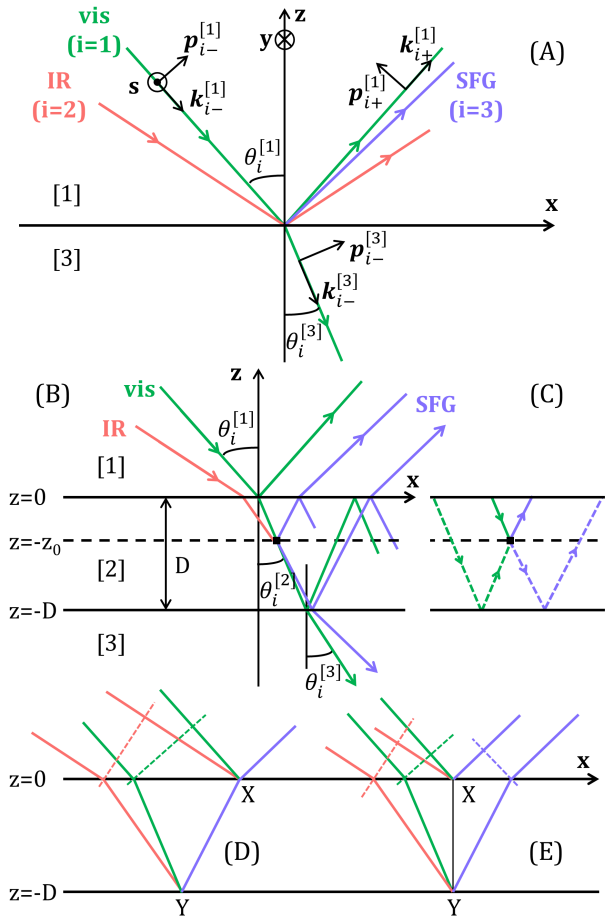

FIG. 1. Sketch of the interface and the SFG process (A) in the two-layer model and (B) in the film model. Only a few reflected, refracted and transmitted rays are shown for clarity. (C) Scheme showing the equal phase delays of incoming and emitted beams. Phase delay calculation (D) according to Ref. 33 and (E) in the present work.

field amplitudes E, wavevectors k) in the following way: subscripts incorporate s/p polarizations, beam number ($i = 1, 2, 3$) and component ($\alpha_i = x, y, z$), whereas superscripts focus on the medium $k = \{1 \cdots N\}$ where the quantity is evaluated. For reflection and transmission coefficients, superscript (ij) means that beam travels from i towards j. The beam number subscript will be skipped every time it is possible without ambiguity.

B. The two-layer model

The simplest system to be considered, involving a plane interface, is composed of two semi-infinite bulk media sharing an interface plane, as in Fig. 1(A). Reviewing this simple

system allows to introduce the key notions and smoothly shift to the film case afterwards. We set at $z = 0$ the $(\boldsymbol{x}, \boldsymbol{y})$ plane defining the interface between the two media numbered [1] ($z>0$, refractive index $n^{[1]}$) and [3] ($z<0$, $n^{[3]}$). Two plane wave monochromatic beams with angular frequencies ω_1 and ω_2, defined by their electric far fields $\boldsymbol{E}^0(\omega_1)$ and $\boldsymbol{E}^0(\omega_2)$ and propagating in $(\boldsymbol{x},\boldsymbol{z})$ plane from medium [1] with wavevectors $\boldsymbol{k}_{1-}^{[1]}$ and $\boldsymbol{k}_{2-}^{[1]}$, overlap on the interface with angles of incidence $\theta_1^{[1]}$ and $\theta_2^{[1]}$. The incident electric fields are naturally decomposed along the $(\boldsymbol{s}, \boldsymbol{p}_-^{[1]})$ bases as defined on Fig. 1(A), with far field amplitudes $E_s^0(\omega_i)$ and $E_p^0(\omega_i)$, respectively. We consider the surface polarization source $\boldsymbol{P}^{[1]}$ located at the interface in medium [1] (i.e. at $z = 0^+$), produced by second-order nonlinear interaction and oscillating at angular frequency $\omega_3 = \omega_1 + \omega_2$. "Surface" polarization means that it derives from a bulk polarization $\boldsymbol{P}_{bulk}^{[1]}$ and is defined as $\boldsymbol{P}_{bulk}^{[1]}(\omega_3, x, y, z) = \boldsymbol{P}^{[1]}(\omega_3, x, y)\delta(z)$. In practical applications, molecules located at $z = 0^+$ or $z = 0^-$ may act as the source of this nonlinear polarization and $\boldsymbol{P}^{[1]}(\omega_3, x, y) \equiv \boldsymbol{P}^{[1]}(\omega_3)$ is a uniform polarization sheet in the $(\boldsymbol{x},\boldsymbol{y})$ plane. We summarize here the results detailed in Ref. 25, reduced to this simplified frame. At this stage, we skip the propagation phases $e^{-i\omega t+i\boldsymbol{k}\cdot\boldsymbol{r}}$ to deal only with amplitudes of the vector fields. The incoming fields $\boldsymbol{E}^{[1]}(\omega_i)$ at the interface are the sum of the downward incident ($\boldsymbol{k}_-^{[1]}$, $\boldsymbol{s}$, $\boldsymbol{p}_-^{[1]}$) and upward reflected ($\boldsymbol{k}_+^{[1]}$, $\boldsymbol{s}$, $\boldsymbol{p}_+^{[1]}$) fields, so that the s and p amplitudes are

$$E_s^{[1]}(\omega_i) = [1 + r_s^{13}(\omega_i)]\boldsymbol{s} \cdot \boldsymbol{E}^0(\omega_i) \tag{1}$$

$$E_p^{[1]}(\omega_i) = [\boldsymbol{p}_{i-}^{[1]} + r_p^{13}(\omega_i)\boldsymbol{p}_{i+}^{[1]}] \cdot \boldsymbol{E}^0(\omega_i) \tag{2}$$

leading, for the components along ($\boldsymbol{x}$, $\boldsymbol{y}$, $\boldsymbol{z}$), to

$$\begin{aligned} E_x^{[1]}(\omega_i) &= E_p^0(\omega_i)[1 - r_p^{13}(\omega_i)] \cos\theta_i^{[1]} \\ E_y^{[1]}(\omega_i) &= -E_s^0(\omega_i)[1 + r_s^{13}(\omega_i)] \\ E_z^{[1]}(\omega_i) &= E_p^0(\omega_i)[1 + r_p^{13}(\omega_i)] \sin\theta_i^{[1]} \end{aligned} \tag{3}$$

In these formulas, reflection coefficients r_p^{13} and r_s^{13} modulate the electric field amplitude of a p-polarized and s-polarized, respectively, electromagnetic wave travelling from [1] to [3] and reflected by the interface.

$$r_s^{13}(\omega_i) = \frac{n_i^{[1]} \cos\theta_i^{[1]} - n_i^{[3]} \cos\theta_i^{[3]}}{n_i^{[1]} \cos\theta_i^{[1]} + n_i^{[3]} \cos\theta_i^{[3]}} \tag{4}$$

$$r_p^{13}(\omega_i) = \frac{n_i^{[3]} \cos\theta_i^{[1]} - n_i^{[1]} \cos\theta_i^{[3]}}{n_i^{[3]} \cos\theta_i^{[1]} + n_i^{[1]} \cos\theta_i^{[3]}} \tag{5}$$

where $\theta_i^{[3]}$ follows from Snell's law $n_i^{[1]} \sin\theta_i^{[1]} = n_i^{[3]} \sin\theta_i^{[3]}$. In a compact form, assuming that incoming electric fields are polarized along a unit vector $\boldsymbol{e}^{[1]}(\omega_i)$ in their ($\boldsymbol{s}$, $\boldsymbol{p}_{i-}^{[1]}$) plane, Eq. 3 transforms into:

$$E_\alpha^{[1]}(\omega_i) = F_\alpha^{2L}(\omega_i) E^0(\omega_i) \left[\boldsymbol{e}^{[1]}(\omega_i) \cdot \boldsymbol{\alpha}\right] = F_\alpha^{2L}(\omega_i) e_\alpha^{[1]}(\omega_i) E^0(\omega_i) \tag{6}$$

where the coefficients linking the local field at the interface $E^{[1]}$ and the far field E^0 are the two layer Fresnel factors:

$$\begin{aligned}
F_x^{2L}(\omega_i) &= [1 - r_p^{13}(\omega_i)] = \frac{2n_i^{[1]} \cos\theta_i^{[3]}}{n_i^{[1]} \cos\theta_i^{[3]} + n_i^{[3]} \cos\theta_i^{[1]}} \\
F_y^{2L}(\omega_i) &= [1 + r_s^{13}(\omega_i)] = \frac{2n_i^{[1]} \cos\theta_i^{[1]}}{n_i^{[1]} \cos\theta_i^{[1]} + n_i^{[3]} \cos\theta_i^{[3]}} \\
F_z^{2L}(\omega_i) &= [1 + r_p^{13}(\omega_i)] = \frac{2n_i^{[3]} \cos\theta_i^{[1]}}{n_i^{[1]} \cos\theta_i^{[3]} + n_i^{[3]} \cos\theta_i^{[1]}}
\end{aligned} \tag{7}$$

The electric field emitted by an arbitrary surface polarization source $\boldsymbol{P}^{[1]}$ is obtained by solving the Maxwell equations at the interface.[9,10,25] The result is remarkably simple[10] as one obtains, when the surface polarization is first simply placed in medium [1] without account of the interface:

$$\boldsymbol{E}^0(\omega_3) = \frac{2i\pi(\omega_3)^2}{c^2 k_{3,z}^{[1]}} \boldsymbol{P}_T^{[1]} \tag{8}$$

where subscript T refers to the transverse component of the nonlinear polarization, that is its projection onto the plane perpendicular to the wavevector, and $k_{3,z}^{[1]} = \frac{\omega_3}{c} n_3^{[1]} \cos\theta_3^{[1]}$ is the component of the SFG wavevector perpendicular to the interface. Here, angle $\theta_3^{[1]}$ follows from the phase matching condition, i.e. conservation of the wavevector components parallel to the interface:

$$n_1^{[1]} \omega_1 \sin\theta_1^{[1]} + n_2^{[1]} \omega_2 \sin\theta_2^{[1]} = n_3^{[1]} \omega_3 \sin\theta_3^{[1]} \tag{9}$$

With explicit addition of the interface, the total field emitted towards medium [1] ($\boldsymbol{k}_{3+}^{[1]}$, $\boldsymbol{s}$, $\boldsymbol{p}_{3+}^{[1]}$) sums up a wave emitted upwards ($\boldsymbol{k}_{3+}^{[1]}$) and one downwards reflected by the interface ($\boldsymbol{k}_{3-}^{[1]}$), with amplitudes for the s and p components:[10,25]

$$E_s^0(\omega_3) = \frac{2i\pi\omega_3^2}{c^2 k_{3,z}^{[1]}} [1 + r_s^{13}(\omega_3)] \boldsymbol{s}.\boldsymbol{P}^{[1]} \tag{10}$$

$$E_p^0(\omega_3) = \frac{2i\pi\omega_3^2}{c^2 k_{3,z}^{[1]}} [\boldsymbol{p}_{3+}^{[1]} + r_p^{13}(\omega_3) \boldsymbol{p}_{3-}^{[1]}].\boldsymbol{P}^{[1]} \tag{11}$$

The s and p components of the emitted electric field appear proportional to the corresponding components of the nonlinear polarization source. Apart from the sign change in x component, the nonlinear polarization behaves like the incoming electric far fields as far as Fresnel factors are concerned, as

$$\begin{aligned} E_s^0(\omega_3) &= -\frac{2i\pi\omega_3}{cn_3^{[1]}\cos\theta_3^{[1]}} P_y^{[1]}[1+r_s^{13}(\omega_3)] \\ E_p^0(\omega_3) &= \frac{2i\pi\omega_3}{cn_3^{[1]}\cos\theta_3^{[1]}} \left(-P_x^{[1]}[1-r_p^{13}(\omega_3)]\cos\theta_3^{[1]} + P_z^{[1]}[1+r_p^{13}(\omega_3)]\sin\theta_3^{[1]}\right) \end{aligned} \tag{12}$$

or, for an emitted field aligned along an arbitrary vector $\boldsymbol{e}^{[1]}(\omega_3)$ in the $(\boldsymbol{s}, \boldsymbol{p}_{3+}^{[1]})$ plane:

$$E^0(\omega_3) = \frac{2i\pi\omega_3}{cn_3^{[1]}\cos\theta_3^{[1]}} \sum_\alpha F_\alpha^{2L}(\omega_3) e_\alpha^{[1]}(\omega_3) P_\alpha^{[1]}(\omega_3) \tag{13}$$

Introducing the surface second order nonlinear susceptibility tensor $\chi^{(2)}$ in the $(\boldsymbol{x}, \boldsymbol{y}, \boldsymbol{z})$ basis as $P_\alpha^{[1]}(\omega_3) = \sum_{\beta\gamma} \chi_{\alpha\beta\gamma}^{(2)} E_\beta^{[1]}(\omega_1) E_\gamma^{[1]}(\omega_2)$ and using

$$I(\omega_i) = \frac{cn_i^{[1]}}{2\pi} \|\boldsymbol{E}^0(\omega_i)\|^2 \tag{14}$$

we finally recover the classical formula for the SFG intensity emitted in the reflection geometry:[26]

$$I_R(\omega_3) = \frac{8\pi^3(\omega_3)^2}{c^3 n_3^{[1]} n_1^{[1]} n_2^{[1]} (\cos\theta_3^{[1]})^2} |\chi_{eff}^{(2)}|^2 I(\omega_1) I(\omega_2) \tag{15}$$

with the definition of the effective surface susceptibility:

$$\chi_{eff}^{(2)} = \sum_{\alpha\beta\gamma} F_\alpha^{2L}(\omega_3) e_\alpha^{[1]}(\omega_3)\, F_\beta^{2L}(\omega_1) e_\beta^{[1]}(\omega_1)\, F_\gamma^{2L}(\omega_2) e_\gamma^{[1]}(\omega_2)\, \chi_{\alpha\beta\gamma}^{(2)} \tag{16}$$

The 2L-model applies of course when the system is strictly speaking composed of only two media (e.g. surface SFG contribution at the air-water or air-metal interfaces) with no change of the bulk optical properties close to the interface. It also applies when a third intermediate layer is added to the system, with vanishing thickness, as long as its optical properties (essentially its refractive index) do not differ from those of one of the bulk media. This is seldom the case in practice because a large proportion of SFG literature deals with the *in situ* analysis of molecular monolayers at interfaces. Of course, one may as a first approximation neglect the molecular refractive index, but in most situations this remains an oversimplification.

III. SYSTEMS WITH TWO INTERFACES

We now introduce an intermediate layer [2] in the system, as in Fig. 1(B), defined between $z = 0$ and $z = -D$, with its own refractive index $n_i^{[2]}$. We first list all the changes to implement to the previous results in order to account for the presence of this layer for an arbitrary thickness D, then turn to two special cases, namely negligible thickness (leading to the three-layer model) and macroscopic thickness. The nonlinear process now takes place at an arbitrary depth $z = -z_0$ in layer [2], where we place the nonlinear polarization sheet, defined as

$$\boldsymbol{P}_{bulk}^{[2]}(\omega_3, x, y, z) = \boldsymbol{P}^{[2]}(\omega_3)\delta(z + z_0) \tag{17}$$

Consequently, the nonlinear susceptibility is now defined as a function of electric fields and polarization evaluated in layer [2]:

$$P_\alpha^{[2]}(\omega_3) = \sum_{\beta\gamma} \chi_{\alpha\beta\gamma}^{(2)} E_\beta^{[2]}(\omega_1, z_0) E_\gamma^{[2]}(\omega_2, z_0) \tag{18}$$

In parallel, the phases arising from wave propagation cannot be neglected, and the electric fields traveling in medium [2] carry a position-dependent phase term $e^{-i\omega_i t + i\boldsymbol{k}_i^{[2]}\cdot\boldsymbol{r}}$. The amplitudes don't add up in phase anymore, leading to interference effects. The amplitude of the SFG response now depends on film thickness D and on depth $z = -z_0$ through phase factors for which the origin is taken at $z = 0$. The incoming fields, as well as the reflected field emitted towards medium [1], are the sum of a downward field (wavevector $k_{i-}^{[2]}$) and an upward field (wavevector $k_{i+}^{[2]}$) reflected by the $\{23\}$ interface. In addition, all beams experiment multiple reflections and transmissions on the boundaries of layer [2], oscillating as in the cavity of a Fabry-Pérot etalon. The process being phase-matched as for the wavevector components parallel to the interface,[8] only dephasing along z matters. We define for beam i the amplitude $k_{i,z}^{[2]}$ of the perpendicular wavevector in medium [2] as $k_{i,z}^{[2]} = \dfrac{\omega_i}{c} n_i^{[2]} \cos\theta_i^{[2]}$, and $\beta_i = k_{i,z}^{[2]} D$ the phase acquired after traveling from $z_0 = 0$ to $z_0 = D$. The derivation in Ref. 25 accounts for all these effects.

A. Reflection geometry

The following changes apply to the three fields fields inside layer [2], modifying Eq. 3 and 12 (see Ref. 25 for more details): (i) incoming fields cross the $\{12\}$ interface (factor $t_{s/p}^{12}$);

(ii) reflected SFG field crosses the {21} interface (factor $t_{s/p}^{21}$); (iii) in Eq. 12, the emission coefficient becomes $\dfrac{2i\pi\omega_3}{cn_3^{[2]}\cos\theta_3^{[2]}}$; (iv) projections onto the ($\boldsymbol{x}$, $\boldsymbol{y}$, $\boldsymbol{z}$) basis rely on angles $\theta_i^{[2]}$ (resp. $\theta_i^{[1]}$), depending on the medium in which the projected quantities are evaluated; (v) phase factors are introduced: $e^{ik_{i,z}^{[2]}z_0}$ for the downward contribution and $e^{2i\beta_i}e^{-ik_{i,z}^{[2]}z_0}$ for the upward one (corresponding to the phase delay needed by each beam to reach the reference $z = 0$ plane); (vi) the Fabry-Pérot effect involves interferences between identical beams phase-shifted by $2k_{i,z}^{[2]}D$, leading to an overall multiplicative factor $1/(1 - r_{s/p}^{21}r_{s/p}^{23}e^{2i\beta_i})$.

For the incoming fields, Eq. 3 becomes:

$$\begin{aligned}
E_x^{[2]}(\omega_i, z_0) &= E_p^0(\omega_i)\frac{t_p^{12}(\omega_i)[e^{ik_{i,z}^{[2]}z_0} - r_p^{23}(\omega_i)e^{2i\beta_i}e^{-ik_{i,z}^{[2]}z_0}]}{1 - r_p^{21}(\omega_i)r_p^{23}(\omega_i)e^{2i\beta_i}}\cos\theta_i^{[2]} \\
E_y^{[2]}(\omega_i, z_0) &= -E_s^0(\omega_i)\frac{t_s^{12}(\omega_i)[e^{ik_{i,z}^{[2]}z_0} + r_s^{23}(\omega_i)e^{2i\beta_i}e^{-ik_{i,z}^{[2]}z_0}]}{1 - r_s^{21}(\omega_i)r_s^{23}(\omega_i)e^{2i\beta_i}} \\
E_z^{[2]}(\omega_i, z_0) &= E_p^0(\omega_i)\frac{t_p^{12}(\omega_i)[e^{ik_{i,z}^{[2]}z_0} + r_p^{23}(\omega_i)e^{2i\beta_i}e^{-ik_{i,z}^{[2]}z_0}]}{1 - r_p^{21}(\omega_i)r_p^{23}(\omega_i)e^{2i\beta_i}}\sin\theta_i^{[2]}
\end{aligned} \tag{19}$$

The definition of the Fresnel factors to use in Eq. 18 is adapted from Eq. 6 as $E_\alpha^{[2]}(\omega_i, z_0) = F_\alpha^{film}(\omega_i)e_\alpha^{[1]}(\omega_i)E^0(\omega_i)$ and we get

$$F_x^{film}(\omega_i) = \frac{t_p^{12}(\omega_i)[e^{ik_{i,z}^{[2]}z_0} - r_p^{23}(\omega_i)e^{2i\beta_i}e^{-ik_{i,z}^{[2]}z_0}]}{1 - r_p^{21}(\omega_i)r_p^{23}(\omega_i)e^{2i\beta_i}}\frac{\cos\theta_i^{[2]}}{\cos\theta_i^{[1]}} \tag{20}$$

$$F_y^{film}(\omega_i) = \frac{t_s^{12}(\omega_i)[e^{ik_{i,z}^{[2]}z_0} + r_s^{23}(\omega_i)]e^{2i\beta_i}e^{-ik_{i,z}^{[2]}z_0}]}{1 - r_s^{21}(\omega_i)r_s^{23}(\omega_i)e^{2i\beta_i}} \tag{21}$$

$$F_z^{film}(\omega_i) = \frac{t_p^{12}(\omega_i)[e^{ik_{i,z}^{[2]}z_0} + r_p^{23}(\omega_i)e^{2i\beta_i}e^{-ik_{i,z}^{[2]}z_0}]}{1 - r_p^{21}(\omega_i)r_p^{23}(\omega_i)e^{2i\beta_i}}\frac{\sin\theta_i^{[2]}}{\sin\theta_i^{[1]}} \tag{22}$$

To recover a more usual form, we transform these expressions using

$$\begin{aligned}
t_p^{12}(\omega_i)\cos\theta_i^{[2]} &= \left[1 - r_p^{12}(\omega_i)\right]\cos\theta_i^{[1]} \\
t_s^{12}(\omega_i) &= \left[1 + r_s^{12}(\omega_i)\right] \\
t_p^{12}(\omega_i)\sin\theta_i^{[2]} &= \left[1 + r_p^{12}(\omega_i)\right]\left(\frac{n_i^{[1]}}{n_i^{[2]}}\right)^2\sin\theta_i^{[1]},
\end{aligned} \tag{23}$$

leading to:

$$F_x^{film}(\omega_i) = e^{ik_{i,z}^{[2]}z_0}\left[1 - r_p^{12}(\omega_i)\right]\frac{1 - r_p^{23}(\omega_i)e^{2i(\beta_i - k_{i,z}^{[2]}z_0)}}{1 + r_p^{12}(\omega_i)r_p^{23}(\omega_i)e^{2i\beta_i}} \tag{24}$$

$$F_y^{film}(\omega_i) = e^{ik_{i,z}^{[2]}z_0}\left[1+r_s^{12}(\omega_i)\right]\frac{1+r_s^{23}(\omega_i)e^{2i(\beta_i-k_{i,z}^{[2]}z_0)}}{1+r_s^{12}(\omega_i)r_s^{23}(\omega_i)e^{2i\beta_i}} \tag{25}$$

$$F_z^{film}(\omega_i) = e^{ik_{i,z}^{[2]}z_0}\left[1+r_p^{12}(\omega_i)\right]\frac{1+r_p^{23}(\omega_i)e^{2i(\beta_i-k_{i,z}^{[2]}z_0)}}{1+r_p^{12}(\omega_i)r_p^{23}(\omega_i)e^{2i\beta_i}}\left(\frac{n_i^{[1]}}{n_i^{[2]}}\right)^2 \tag{26}$$

We recognize in these expressions the four contributions to Fresnel factors in the film model: (i) a global phase factor, common to all polarizations, accounting for beam propagation into the film from the first interface to z_0; (ii) a usual reflectivity coefficient at the $\{12\}$ interface; (iii) a Fabry-Pérot term describing the multiple beam reflections and interferences inside medium [2], resulting in the sum of a downward wave and an upward wave; (iv) the continuity conditions of the parallel electric and perpendicular displacement fields (see below Part. III D 1 for a discussion).

For the emitted SFG field, Eq. 12 transforms into:

$$E_s^0(\omega_3) = -\frac{2i\pi\omega_3}{cn_3^{[2]}\cos\theta_3^{[2]}}\frac{t_s^{21}(\omega_3)[e^{ik_{3,z}^{[2]}z_0}+r_s^{23}(\omega_3)e^{2i\beta_3}e^{-ik_{3,z}^{[2]}z_0}]}{1-r_s^{21}(\omega_3)r_s^{23}(\omega_3)e^{2i\beta_3}}P_y^{[2]} \tag{27}$$

$$\begin{aligned}E_p^0(\omega_3) = \frac{2i\pi\omega_3 t_p^{21}(\omega_3)}{cn_3^{[2]}\cos\theta_3^{[2]}}\Bigg(&-P_x^{[2]}\frac{e^{ik_{3,z}^{[2]}z_0}-r_p^{23}(\omega_3)e^{2i\beta_3}e^{-ik_{3,z}^{[2]}z_0}}{1-r_p^{21}(\omega_3)r_p^{23}(\omega_3)e^{2i\beta_3}}\cos\theta_3^{[2]}\\&+P_z^{[2]}\frac{e^{ik_{3,z}^{[2]}z_0}+r_p^{23}(\omega_3)e^{2i\beta_3}e^{-ik_{3,z}^{[2]}z_0}}{1-r_p^{21}(\omega_3)r_p^{23}(\omega_3)e^{2i\beta_3}}\sin\theta_3^{[2]}\Bigg)\end{aligned} \tag{28}$$

These expressions simplify using Eq. 23, together with:

$$\frac{1}{n_3^{[2]}\cos\theta_3^{[2]}}t_{s/p}^{21}(\omega_3) = \frac{1}{n_3^{[1]}\cos\theta_3^{[1]}}t_{s/p}^{12}(\omega_3) \tag{29}$$

to recover the same factors as in Eqs. 19 and get

$$E^0(\omega_3) = \frac{2i\pi\omega_3}{cn_3^{[1]}\cos\theta_3^{[1]}}\sum_\alpha F_\alpha^{film}(\omega_3)e_\alpha^{[1]}(\omega_3)P_\alpha^{[2]}(\omega_3) \tag{30}$$

using for $F_\alpha^{film}(\omega_3)$ the same formulas as for $i=1,2$ (Eqs. 24-26). In the end, we see that Eq. 15 is still valid while Eq. 16 is only modified by simply changing superscripts "2L" to "film":

$$\chi_{eff}^{(2)} = \sum_{\alpha\beta\gamma} F_\alpha^{film}(\omega_3)e_\alpha^{[1]}(\omega_3)\,F_\beta^{film}(\omega_1)e_\beta^{[1]}(\omega_1)\,F_\gamma^{film}(\omega_2)e_\gamma^{[1]}(\omega_2)\,\chi_{\alpha\beta\gamma}^{(2)} \tag{31}$$

Switching from two-layer model to thin film model involving interferences thus entirely rests on the modification of the Fresnel factors. Still, we find that these remain identical for the

three beams even in this configuration for arbitrary depth z_0. This result is in fact very general as will be discussed in details in Part III D 2 below.

Most applications encountered in the literature focus on the particular cases $z_0 = 0$ and $z_0 = D$ (an example of a general description for arbitrary z_0 may be found in Ref. 19). For the sake of completeness, we explicit the expressions of the Fresnel factors in these situations.

$$F_x^{film}(z_0 = 0) = \left[1 - r_p^{12}(\omega_i)\right] \frac{1 - r_p^{23}(\omega_i) e^{2i\beta_i}}{1 + r_p^{12}(\omega_i) r_p^{23}(\omega_i) e^{2i\beta_i}} \tag{32}$$

$$F_y^{film}(z_0 = 0) = \left[1 + r_s^{12}(\omega_i)\right] \frac{1 + r_s^{23}(\omega_i) e^{2i\beta_i}}{1 + r_s^{12}(\omega_i) r_s^{23}(\omega_i) e^{2i\beta_i}} \tag{33}$$

$$F_z^{film}(z_0 = 0) = \left[1 + r_p^{12}(\omega_i)\right] \frac{1 + r_p^{23}(\omega_i) e^{2i\beta_i}}{1 + r_p^{12}(\omega_i) r_p^{23}(\omega_i) e^{2i\beta_i}} \left(\frac{n_i^{[1]}}{n_i^{[2]}}\right)^2 \tag{34}$$

Here all the activity happens at the upper interface, where the phase shift between downward and upward bouncing beams is maximal. The presence of the film is equivalent to a mere modification of the total reflectivity of the system. Hence, we can write:

$$F_x^{film}(z_0 = 0) = 1 - r_p^{123}(\omega_i) = 1 - \frac{r_p^{12}(\omega_i) + r_p^{23}(\omega_i) e^{2i\beta_i}}{1 + r_p^{12}(\omega_i) r_p^{23}(\omega_i) e^{2i\beta_i}} \tag{35}$$

$$F_y^{film}(z_0 = 0) = 1 + r_s^{123}(\omega_i) = 1 + \frac{r_s^{12}(\omega_i) + r_s^{23}(\omega_i) e^{2i\beta_i}}{1 + r_s^{12}(\omega_i) r_s^{23}(\omega_i) e^{2i\beta_i}} \tag{36}$$

$$F_z^{film}(z_0 = 0) = \left[1 + r_p^{123}(\omega_i)\right] \left(\frac{n_i^{[1]}}{n_i^{[2]}}\right)^2 = \left[1 + \frac{r_p^{12}(\omega_i) + r_p^{23}(\omega_i) e^{2i\beta_i}}{1 + r_p^{12}(\omega_i) r_p^{23}(\omega_i) e^{2i\beta_i}}\right] \left(\frac{n_i^{[1]}}{n_i^{[2]}}\right)^2 \tag{37}$$

where $r_{s/p}^{123}(\omega_i)$ is the reflectivity of the complete three-layer system[14,34], which converges to $r_{s/p}^{13}(\omega_i)$ when $D \to 0$.

For $z_0 = D$, i.e. $\beta_i - k_{i,z}^{[2]} z_0 = 0$:

$$F_x^{film}(z_0 = D) = e^{i\beta_i} \left[1 - r_p^{12}(\omega_i)\right] \frac{1 - r_p^{23}(\omega_i)}{1 + r_p^{12}(\omega_i) r_p^{23}(\omega_i) e^{2i\beta_i}} \tag{38}$$

$$F_y^{film}(z_0 = D) = e^{i\beta_i} \left[1 + r_s^{12}(\omega_i)\right] \frac{1 + r_s^{23}(\omega_i)}{1 + r_s^{12}(\omega_i) r_s^{23}(\omega_i) e^{2i\beta_i}} \tag{39}$$

$$F_z^{film}(z_0 = D) = e^{i\beta_i} \left[1 + r_p^{12}(\omega_i)\right] \frac{1 + r_p^{23}(\omega_i)}{1 + r_p^{12}(\omega_i) r_p^{23}(\omega_i) e^{2i\beta_i}} \left(\frac{n_i^{[1]}}{n_i^{[2]}}\right)^2 \tag{40}$$

Here, on the contrary, there is no phase shift between downward and upward beams, as can be seen on Figure 1(B), leading to a common global phase β_i. In this particular case, the

result is easily extended to the situation where the nonlinear source at $z_0 = D$ is placed into medium [3] rather than medium [2] (for example originating from the buried substrate): only F_z^{film} must be further multiplied by $(n_i^{[2]}/n_i^{[3]})^2$ in order to account for the continuity of the displacement field at the $\{23\}$ interface.[12]

In our formalism, universality of the Fresnel factors for the three beams in equations (24)-(26) is enforced, whatever the location $z = -z_0$ of the nonlinear sheet. Universality is surprisingly not always implemented in the literature dealing with thick films.[5,11–13,19,33,35] In particular, when SFG produced at $z_0 = D$ is analyzed, the phase shifts called Δ_i take different forms for the three beams, introducing an unnecessary complication. This is easily understood when considering these original phase calculations as sketched on Figure 1(D). The phases are calculated by evaluating the differences in path lengths between the "direct" process at $z_0 = 0$ (point X), and the "buried" process at $z_0 = D$ (point Y). These phases encompass a superfluous contribution parallel to the interface because the two interacting points don't share a common x coordinate. In fact, the phases alone for each Fresnel factor don't have an absolute meaning, as only the overall phase $\Delta_1 + \Delta_2 + \Delta_3$ is meaningful. It can be checked that this overall phase simplifies from the extra terms when plugging in the phase matching condition $k_{1,||}^{[1]} + k_{2,||}^{[1]} = k_{3,||}^{[1]}$ (Eq. 9). In our formalism (Figure 1(E)), the two interacting points are aligned on a vertical line, which allows to restore the symmetry between incoming and emitted beams, and introduces no extra parallel term. In these conditions, it is easy to show that the three phase delays between direct and buried processes all have the same value for the three beams $\Delta_i = \dfrac{\omega_i D}{c}(n_i^{[2]}/\cos\theta_i^{[2]} - n_i^{[1]}\tan\theta_i^{[2]}\sin\theta_i^{[1]}) = \dfrac{\omega_i D}{c} n_i^{[2]}\cos\theta_i^{[2]} = \beta_i$.

Interestingly, the global phase Δ_R due to beam propagation at arbitrary location $z = -z_0$ is equal to

$$\Delta_R(z = -z_0) = [k_{1,z}^{[2]} + k_{2,z}^{[2]} + k_{3,z}^{[2]}]\, z_0, \tag{41}$$

in other words we recover for Δ_R the (positive) phase mismatch of the SFG process at depth $-z_0$ between the three beams in reflection geometry $\Delta_R = (\Delta k_{z,R}^{[2]})\, z_0$.

B. Transmission geometry

Using again Ref. 25 as a guide, we may list the transformations to implement into the previous equations in order to calculate the Fresnel factors at arbitrary depth $z = -z_0$ for

SFG emitted in the transmission geometry (i.e. into medium [3]). The SFG factors $F(\omega_3)$ may not this time remain equal to the incoming ones $F(\omega_{1,2})$, as $F(\omega_3)$ now accounts for the transfer from the far field in medium [3] to medium [2]. It may be inferred that equations (20)-(22) transform by : i) replacing $t_{s,p}^{12}(\omega_i)$ by $t_{s,p}^{23}(\omega_i)$; ii) inverting the roles of $r_{s,p}^{21}(\omega_i)$ and $r_{s,p}^{23}(\omega_i)$; iii) changing sine and cosine projections from medium [1] to medium [3]; iv) modifying the phase factors by calculating the positive phase from $z = -z_0$ to $z = -D$ and subtracting the phase advance of plane $z = -D$, equal to $k_{3,z}^{[2]}D$, with respect to the phase reference plane $z = 0$. This leads to phase factors equal to $e^{-ik_{3,z}^{[2]}z_0}$ and $e^{ik_{3,z}^{[2]}z_0}$ for the downward and upward beams, respectively. Accordingly, we modify Eq. (31) into

$$\chi_{eff,T}^{(2)} = \sum_{\alpha\beta\gamma} F_\alpha^{film,T}(\omega_3) e_\alpha^{[3]}(\omega_3)\, F_\beta^{film}(\omega_1) e_\beta^{[1]}(\omega_1)\, F_\gamma^{film}(\omega_2) e_\gamma^{[1]}(\omega_2)\, \chi_{\alpha\beta\gamma}^{(2)} \tag{42}$$

and the emission coefficient in Eq. (30) into $\dfrac{2i\pi\omega_3}{cn_3^{[3]}\cos\theta_3^{[3]}}$, leading to a transmitted intensity

$$I_T(\omega_3) = \frac{8\pi^3(\omega_3)^2}{c^3 n_3^{[3]} n_1^{[1]} n_2^{[1]} (\cos\theta_3^{[3]})^2} |\chi_{eff,T}^{(2)}|^2 I(\omega_1) I(\omega_2). \tag{43}$$

As a result, the transmission Fresnel coefficients are:

$$F_x^{film,T}(\omega_3) = e^{-ik_{3,z}^{[2]}z_0} \left[1 - r_p^{32}(\omega_3)\right] \frac{1 - r_p^{21}(\omega_3) e^{2i(k_{3,z}^{[2]}z_0)}}{1 + r_p^{32}(\omega_3) r_p^{21}(\omega_3) e^{2i\beta_3}} \tag{44}$$

$$F_y^{film,T}(\omega_3) = e^{-ik_{3,z}^{[2]}z_0} \left[1 + r_s^{32}(\omega_3)\right] \frac{1 + r_s^{21}(\omega_3) e^{2i(k_{3,z}^{[2]}z_0)}}{1 + r_s^{32}(\omega_3) r_s^{21}(\omega_3) e^{2i\beta_3}} \tag{45}$$

$$F_z^{film,T}(\omega_3) = e^{-ik_{3,z}^{[2]}z_0} \left[1 + r_p^{32}(\omega_3)\right] \frac{1 + r_p^{21}(\omega_3) e^{2i(k_{3,z}^{[2]}z_0)}}{1 + r_p^{32}(\omega_3) r_p^{21}(\omega_3) e^{2i\beta_3}} \left(\frac{n_3^{[3]}}{n_3^{[2]}}\right)^2 \tag{46}$$

For arbitrary depth $z = -z_0$, the global phase becomes

$$\Delta_T(z = -z_0) = [k_{1,z}^{[2]} + k_{2,z}^{[2]} - k_{3,z}^{[2]}]\, z_0, \tag{47}$$

and we recover for Δ_T the SFG phase mismatch between the three beams in transmission geometry $\Delta_T = (\Delta k_{z,T}^{[2]})\, z_0$.

For completeness, the coefficients at the boundaries become:

$$F_x^{film,T}(z_0 = 0) = \left[1 - r_p^{32}(\omega_3)\right] \frac{1 - r_p^{21}(\omega_3)}{1 + r_p^{32}(\omega_3) r_p^{21}(\omega_3) e^{2i\beta_3}} \tag{48}$$

$$F_y^{film,T}(z_0 = 0) = \left[1 + r_s^{32}(\omega_3)\right] \frac{1 + r_s^{21}(\omega_3)}{1 + r_s^{32}(\omega_3) r_s^{21}(\omega_3) e^{2i\beta_3}} \tag{49}$$

$$F_z^{film,T}(z_0=0) = \left[1+r_p^{32}(\omega_3)\right] \frac{1+r_p^{21}(\omega_3)}{1+r_p^{32}(\omega_3)r_p^{21}(\omega_3)e^{2i\beta_3}} \left(\frac{n_3^{[3]}}{n_3^{[2]}}\right)^2 \tag{50}$$

and

$$\begin{aligned} F_x^{film,T}(z_0=D) &= e^{-i\beta_3}\left[1-r_p^{32}(\omega_3)\right] \frac{1-r_p^{21}(\omega_3)e^{2i\beta_3}}{1+r_p^{32}(\omega_3)r_p^{21}(\omega_3)e^{2i\beta_3}} \\ &= e^{-i\beta_3}\left[1-r_p^{321}(\omega_3)\right] \end{aligned} \tag{51}$$

$$\begin{aligned} F_y^{film,T}(z_0=D) &= e^{-i\beta_3}\left[1+r_s^{32}(\omega_3)\right] \frac{1+r_s^{21}(\omega_3)e^{2i\beta_3}}{1+r_s^{32}(\omega_3)r_s^{21}(\omega_3)e^{2i\beta_3}} \\ &= e^{-i\beta_3}\left[1+r_s^{321}(\omega_3)\right] \end{aligned} \tag{52}$$

$$\begin{aligned} F_z^{film,T}(z_0=D) &= e^{-i\beta_3}\left[1+r_p^{32}(\omega_3)\right] \frac{1+r_p^{21}(\omega_3)e^{2i\beta_3}}{1+r_p^{32}(\omega_3)r_p^{21}(\omega_3)e^{2i\beta_3}} \left(\frac{n_3^{[3]}}{n_3^{[2]}}\right)^2 \\ &= e^{-i\beta_3}\left[1+r_p^{321}(\omega_3)\right] \left(\frac{n_3^{[3]}}{n_3^{[2]}}\right)^2 \end{aligned} \tag{53}$$

The behavior is fully symmetric to the reflection case upon exchanging $z_0 = 0$ and $z_0 = D$, i.e. the entrance and exit interfaces. The only difference lies in the global phase factor, for which symmetry is broken as a consequence of the choice of plane $z = 0$ as the common phase reference.

C. Particular cases

The film model above is in principle valid for any thickness, from ultrathin to macroscopic films. However, we may put forward two extreme configurations for which the previous results simplify. For ultrathin layers (including monolayers), all phase differences disappear, leading to the well-known three-layer (3L) model. For macroscopic layers on the other side, phases still play a big role but the existence of the Fabry-Pérot effect becomes questionable.

1. The three-layer model

The three-layer model, widely used to describe molecular monolayers sandwiched between two semi-infinite bulks,[26] follows from the above when quantities D and z_0 converge towards 0. However, it also remains valid for thicker layers when all phase factors may be neglected,

which is achieved when the biggest phase is considered very small, in other words $|k_{3,z}^{[2]}D| \ll 1$, or even $D \ll \lambda_{SFG}/2\pi$ for a usual dielectric medium [2].

The link with the 2L-model does not straightforwardly appear by removing the phase factors in Eqs. 24-26, but is revealed using the following equalities:

$$\frac{[1-r_p^{12}(\omega_i)][1-r_p^{23}(\omega_i)]}{1+r_p^{12}(\omega_i)r_p^{23}(\omega_i)} = \frac{2n_i^{[1]}\cos\theta_i^{[3]}}{n_i^{[1]}\cos\theta_i^{[3]}+n_i^{[3]}\cos\theta_i^{[1]}} = 1-r_p^{13}(\omega_i) \tag{54}$$

$$\frac{[1+r_s^{12}(\omega_i)][1+r_s^{23}(\omega_i)]}{1+r_s^{12}(\omega_i)r_s^{23}(\omega_i)} = \frac{2n_i^{[1]}\cos\theta_i^{[1]}}{n_i^{[1]}\cos\theta_i^{[1]}+n_i^{[3]}\cos\theta_i^{[3]}} = 1+r_s^{13}(\omega_i) \tag{55}$$

$$\frac{[1+r_p^{12}(\omega_i)][1+r_p^{23}(\omega_i)]}{1+r_p^{12}(\omega_i)r_p^{23}(\omega_i)} = \frac{2n_i^{[3]}\cos\theta_i^{[1]}}{n_i^{[1]}\cos\theta_i^{[3]}+n_i^{[3]}\cos\theta_i^{[1]}} = 1+r_p^{13}(\omega_i) \tag{56}$$

Hence, Eqs. 16 transforms into

$$\chi_{eff}^{(2)} = \sum_{\alpha\beta\gamma} F_\alpha^{3L}(\omega_3)e_\alpha^{[1]}(\omega_3)\, F_\beta^{3L}(\omega_1)e_\beta^{[1]}(\omega_1)\, F_\gamma^{3L}(\omega_2)e_\gamma^{[1]}(\omega_2)\, \chi_{\alpha\beta\gamma}^{(2)} \tag{57}$$

with

$$\begin{aligned} F_x^{3L}(\omega_i) &= F_x^{2L}(\omega_i) \\ F_y^{3L}(\omega_i) &= F_y^{2L}(\omega_i) \\ F_z^{3L}(\omega_i) &= F_z^{2L}(\omega_i)\left(\frac{n_i^{[1]}}{n_i^{[2]}}\right)^2 \end{aligned} \tag{58}$$

We recover the well-known result that Fresnel factors in the 2L and 3L models are equal, to the exception of the boundary conditions for z-component at interface $\{12\}$.

Finally, the 2L and 3L-models with vanishing thickness in transmission geometry follow from Eq. (51)-(53) by setting $\beta_3 = 0$ and recalling that $r_{s/p}^{321}(\omega_3) = r_{s/p}^{31}(\omega_3)$ in this situation.

2. Macroscopic layers

The analysis of Parts III A and III B apply as soon as the thickness of the intermediate layers may not be neglected. However, even in this situation, some differences may occur between microscopic (thin) and macroscopic (thick) layers. The equations in those Parts take full account of the Fabry-Pérot (F-P) effect due to interferences between all the beams propagating and bouncing inside layer [2] after multiple reflections at the $\{23\}$ and $\{21\}$ boundaries. This analysis is correct as long as the system allows long range propagation and

overlap of the multiple reflected beams. When layer [2] becomes thick, or even macroscopic, these hypotheses suffer from several restrictions. In practical SFG experiments, these thick layers are in general made of wafers, plates or windows not originally designed for perfect F-P effect, or in any case too thick to perfectly achieve it. It is known that even manufactured F-P resonators may suffer from imperfections, due to non-parallel plane surfaces or non-planar boundaries, either slightly spherical or roughened.[36,37] Quantitatively, the upper bound of the misalignment of two adjacent plane interfaces in the system (i.e. non-parallelism) leading to an incomplete F-P effect is a fraction of the wavelength.[38] It is therefore more easily reached for thick layers, whereas it may be neglected when the thickness of the interfering layer is roughly up to the order of magnitude of the wavelength. In addition, contrary to optical set-ups designed for F-P analysis, SFG experiments usually make use of small and focused beams at high angles of incidence. In these kinds of geometries, it is easy to see that the multiple beams inside a thick layer [2] experiment a drift in position which quickly leads to loss of spatial overlap, all the more as beam overlap is usually experimentally optimized at one of the interfaces, not at the middle of the thick layer. When ultrashort pulses are involved, we may also expect that the pulses, originally overlapped in time, acquire a progressive time delay as a consequence of their different propagation speeds (i.e. group velocities), leading to a decreasing efficiency when multiple reflections are involved. Finally, for gaussian beams, the nonlinear phenomenon essentially takes place close to the overlapping beam centers where the intensities of the input beams are maximal, and the multiple reflected beams quickly shift away from this small optimal zone.

As a consequence, when the film thickness becomes macroscopic (typically for $D \gg \lambda_{IR}$), it seems reasonable to treat macroscopic films in a specific way by adapting the implementation and magnitude of the F-P effect to the experimental geometry and sample properties. In particular, it is conceivable to completely neglect the multiple reflections,[38] still considering a superposition of a downward and an upward beam, with their respective phases. In this case, the applicable Fresnel factors transform from Eq. 24-26 and 44-46 by removing the denominators.

D. Fresnel factors: a central role in surface SFG

Fresnel factor may sometimes be seen as a burden, a mandatory step complicating experimental data analysis. Their relative weights and phases when beam polarizations are tuned, their dispersions in the infrared or visible ranges, the uncertainty on the value of $n_i^{[2]}$ of a monolayer for the evaluation of F_z (sometimes referred to as the n' problem[26,39,40]), even the choice among the various available formulas in the literature, all these traps have a great impact on the transformation of raw SFG data into scientific results, which are not easily appreciated at the time of data recording. However, the inescapable nuisance they introduce in the post-processing should not lead to forget their essential role, their link to the choice of the model for the interface, and their relation to the grounds of SFG emission at the interface. In this part, we review these properties.

1. Transfer factors, boundary conditions and choice of the model

The three fields involved in data analysis (Eq. 15) are experimentally known in the far field in medium [1], whereas the nonlinear susceptibility links the fields and nonlinear polarization ($P_\alpha = \chi^{(2)}_{\alpha\beta\gamma} E_\beta E_\gamma$) evaluated at the interface, where the nonlinear process actually takes place. As the Fresnel factors link the amplitudes of the local fields to those of the corresponding far fields, they are transfer factors from the far fields to the local fields. The 2L-model is the one where all the nonlinear process is defined in medium [1], identically in the film and 3L-models, all quantities are evaluated in medium [2]. For that respect, Eq. 57 plugged into Eq. 15 is somehow misleading because all expressions are written in terms of quantities expressed in media [1] and [3] only ($n_i^{[2]}$ in F_z is the only sign that the nonlinear process is located in medium [2]). Comparing 2L to 3L-model allows understanding the relationship between F^{2L} and F^{3L}: their difference simply expresses the boundary conditions for electric field components between media [1] and [2] (Eq. 54-56). We recover the continuity equation of the parallel components (hence $F^{2L}_{x/y} = F^{3L}_{x/y}$) and that of the perpendicular components of the displacement vector (hence $\varepsilon^{[1]} F^{2L}_z = \varepsilon^{[2]} F^{3L}_z$).[12]

We point out that the choice of the optical model to describe the interface, which essentially comes down to applying a particular set of Fresnel coefficients, has major consequences on the nature of the SFG process itself, and should be made in full knowledge. In fact, for

a film with negligible thickness, it is in principle possible to freely choose in which medium ([1], [2] or [3]) to evaluate the incoming fields and to place the nonlinear polarization. The formulas for Fresnel factors follow accordingly. For that respect, the 3L model allows total flexibility in the choice of evaluation media by simply setting appropriate refractive indices in F_z factors (i.e. adjusting boundary conditions). For example, transforming $n_i^{[2]}$ into $n_i^{[1]}$ in Eq. 58 allows defining the ω_i field in medium [1] and transforms the 3L-model into the 2L-model. Conversely, using $n_i^{[3]}$ instead of $n_i^{[2]}$ places the fields and nonlinear source into substrate [3], allowing to measure its nonlinear response.[41] This situation being equivalent to a 2L model where the nonlinear process all happens in medium [3], Fresnel factors in this case can be noted F^{2L-}.

It is also possible to consider hybrid models for which incoming fields and nonlinear polarization are placed in different layers. The SHG community working on the nonlinear response of solid substrates like metals is used to playing with the definitions of $\chi^{(2)}$ in different media. The appropriate correcting factors are easily included in the microscopic to macroscopic transformations of metal properties.[42,43] This results in substantial differences between numerical values of $\chi^{(2)}$,[44] and sometimes to discrepancies between various publications, but leads to a unique definition of $\chi^{(2)}_{eff}$ as far as the comparison to experimental results is concerned. The SFG community on the other hand is most of the times interested in the molecular layer [2] rather than the substrate itself (with a few exceptions[41,45–47]), therefore concentrating on 2L and 3L models. In some publications, incoming fields are evaluated in medium [2], where the nonlinear process happens, and the nonlinear polarization placed in medium [1], where it is eventually measured.[12,48–50] Finally, the L/K model[30,51] is a hybrid description of the interface where the incoming beams are evaluated in medium [1], and the nonlinear polarization in medium [2]. This peculiar choice does not appear supported by logical grounds. Considering that it has consequences on the definition of the nonlinear susceptibility tensor $\chi^{(2)}$, as we explain here below, it would be advisable to use this model with great care in order to avoid erroneous interpretations.

Turning back to equality $P_\alpha = \chi^{(2)}_{\alpha\beta\gamma} E_\beta E_\gamma$ and considering that the amplitudes of P_α, E_β and E_γ vary with the choice of the medium in which they are evaluated, we see that the value of $\chi^{(2)}_{\alpha\beta\gamma}$ also depends on this choice for the media, thus on the model. The surface nonlinear susceptibility tensor is thus not a universal quantity.[44] Only the far field SFG intensity, and the effective susceptibility in Eq. 15, becomes independent on the models after correction

from Fresnel factors. This may have consequences when the values of $\chi^{(2)}$ components are determined from molecular vibrational properties by *ab initio* methods, for example density functional theory (DFT), or bond additivity model[52–54] and projected onto a local frame in order to deduce molecular orientation from experiments.

In the Supplementary Information of Ref. 55, the authors point out two main differences between the various expressions of the Fresnel factors found in the literature (according to the L/K model and the 3L model, respectively). The first one is the $(n_i^{[1]}/n_i^{[2]})^2$ factor in F_z, and we have seen that it is linked to the choice of the medium ([1] or [2]) to evaluate the fields and the induced polarization. This point is thus attributable to different choices for the definition of $\chi^{(2)}$. The second discrepancy is a missing factor in the L/K model expression of the SFG s-factor. It is explainable by the difference between the 3L model, for which the emission factor $\dfrac{2i\pi(\omega_3)^2}{c^2 k_{3,z}^{[1]}}$ is introduced as in Eq. 8, and the L/K model, which explicitly includes this factor in the Fresnel coefficient for ω_3, leading to a simplification of the excess $n_3^{[1]}\cos\theta_3^{[1]}$. When all mandatory factors are included to recover the expression of the far field (or intensity), taking into account that intensities are also sometimes defined as just the squared field amplitudes, this difference between both models disappears.

2. Universality

Universality of the three Fresnel factors at arbitrary depth z_0 in the film model is an originality of this work. However, it has also long been wondered why, in the 2L and 3L-models, the Fresnel factors for the emitted beam at ω_3 are identical to those for incoming beams at ω_1 and ω_2. In the way they are calculated above, it may look like a fortuitous coincidence in Eq. 23, 29 and 54-56. In particular, it is not obvious why the Fresnel factor for the outgoing beam should be the same as for the incoming ones as (i) the former relates to the nonlinear polarization and the latter to the incoming electric fields; (ii) they relate to beams which don't cross the $\{12\}$ interface in the same direction. The fact is that Fresnel factors are indeed always universal, i.e. identical for the three beams, in the reflection geometry whatever the number of layers (N) of the interface, their thicknesses, the layer $[k]$ and depth where the nonlinear polarization lies, under a few conditions listed below.

There are two ways, internal and external, to understand this. In the internal description, the SFG electric field is calculated as emitted in layer $[k]$ and transferred to the far field in

medium [1], then universality is checked from the result. For the 2L, 3L and film models, the explicit calculation as performed above for x, y and z components allows to recover the universality.

In a finer analysis of this calculation, we may split the SFG emitted field (Eq. 28) in four contributions: (i) emission factor in medium [2], (ii) interface crossing from medium [2] to medium [1], (iii) Fabry-Pérot effect in medium [2], (iv) sum of upward and downward beams. Comparing Eq. 19 and 28 shows that the Fabry-Pérot effect is the same for incoming and outgoing fields. This can be understood by tracing the various rays bouncing inside layer [2], which experiment the same reflection factors whatever the incoming or outgoing nature of the beam. From Fig. 1(C), we also see that the two incoming beams, propagating downwards and upwards, involved in SFG production at the interaction point (black square) have indeed the same phases as the two SFG beams (propagating upwards and downwards, respectively) produced from this point. As for the emission factor and interface crossing, Eq. 29 shows that they are coupled, i.e. the SFG beam emitted in medium [2] and transmitted into medium [1] is equivalent to a beam emitted in medium [1] and transmitted into medium [2]. The emission coefficient is not part of the Fresnel factors, but it has to be explicitly taken into account in the final formulas for the effective susceptibility in order to ensure the coherence of the model and recover the universality in the product of the four contributions. The problem with this internal description is that it requires a calculation of all fields evaluated at the local position of the nonlinear polarization sheet, from which the universality can be checked. For more complex interfaces beyond the film model, this postpones such a proof of universality until the corresponding model is available.

A more general way to show universality is the external point of view.[10] The interface is this time considered as a global object, whatever the number of layers and whatever the layer $[k]$ we place the nonlinear polarization $\boldsymbol{P}^{[k]}$ in. All the elementary entities (e.g. dipoles) composing the interface are located and emit light in medium [1] as in the Ewald-Oseen theorem.[56–59] SFG emission from the nonlinear sheet thus follows the simple rule adapted from Eq. 8:

$$E^0(\omega_3) = \boldsymbol{E}^0(\omega_3) \cdot \boldsymbol{e}^{[1]} = \frac{2i\pi(\omega_3)^2}{c^2 k_{3,z}^{[1]}} \boldsymbol{P}^{[k]} \cdot \boldsymbol{e}^{[k]} \tag{59}$$

The transversality of the emission, translated by the projection onto a transverse vector $\boldsymbol{e}^{[k]}$, means this time that we have to consider all the possible vectors, transverse to a

propagation direction in medium $[k]$, which eventually transform into transverse vector $\boldsymbol{e}^{[1]}$ after traveling across the boundaries from medium $[k]$ to medium [1]. Such vectors are known because they reversely correspond to all the transverse vectors traveling in medium $[k]$ and originating from a single incoming beam with electric far field aligned along unit vector $\boldsymbol{e}^{[1]}$. Calling $F_\alpha^{[k]}$ the transfer factor of the α component from far field to local field in $[k]$, in other words the α component of Fresnel factor $F^{[k]}$, we have

$$E_\alpha^{[k]}(\omega_i) = F_\alpha^{[k]}(\omega_i) E^0(\omega_i) \left[\boldsymbol{e}^{[1]}(\omega_i) \cdot \boldsymbol{\alpha}\right] = F_\alpha^{[k]}(\omega_i) e_\alpha^{[1]}(\omega_i) E^0(\omega_i) \tag{60}$$

whereas field $\boldsymbol{E}^{[k]}$ is also transverse, along vector $\boldsymbol{e}^{[k]}$ defined as

$$E_\alpha^{[k]}(\omega_i) = E^0(\omega_i) \left[\boldsymbol{e}^{[k]}(\omega_i) \cdot \boldsymbol{\alpha}\right] \tag{61}$$

leading to

$$\boldsymbol{e}^{[k]}(\omega_i) \cdot \boldsymbol{\alpha} = F_\alpha^{[k]}(\omega_i) \left[\boldsymbol{e}^{[1]}(\omega_i) \cdot \boldsymbol{\alpha}\right]. \tag{62}$$

$\boldsymbol{e}^{[k]}(\omega_i)$ is not unitary, but defines the transverse propagation of the electric field in medium $[k]$, taking into account all the reflection and refraction processes in-between, in direct relation to its transverse vector $\boldsymbol{e}^{[1]}(\omega_i)$ in the far field. Gathering Eq. 59-62, we finally get

$$E^0(\omega_3) = \frac{2i\pi(\omega_3)^2}{c^2 k_{3,z}^{[1]}} \sum_\alpha P_\alpha^{[k]} F_\alpha^{[k]}(\omega_3) e_\alpha^{[1]} \tag{63}$$

This external formulation show that Fresnel factors are not only transfer factors from the far field to the local field: from the optical point of view, they integrate all the linear optical phenomena happening inside the interface, in other words they "are" the interface.

The uniqueness of the Fresnel factors $F(\omega_3) = F(\omega_{1/2})$ is thus a universal property of SFG emission reflected from any interface. From the proofs above, we see that it relies on several hypotheses: (i) all electric fields are transverse; (ii) the SFG emitted field is proportional to the transverse part of the nonlinear polarization (Eq. 8); (iii) a plane wave description is assumed, ensuring the previous transversality condition; (iv) all fields coupled to tensor $\chi^{(2)}$ must belong to the same medium, hence the natural choice of the 3L-model; (v) the correct emission factor must be factored out in Eq. 8 and 15, as it conditions the value of $F(\omega_3)$.

3. Origin and consequences of transversality

Equation 8, obtained from solving the Maxwell equations at an interface in the presence of an arbitrary polarization source, is at the heart of the modeling of second-order nonlinear

properties at interfaces.[9,10] This important result may be recovered directly by considering the surface nonlinear polarization as a uniform surface density of oscillating dipoles emitting an electric field at ω_3. Considering in a first step a single dipole $\boldsymbol{D}$ at the interface, the emitted field is easily calculated[56] and constitutes the basis of antenna emission. It sums up three terms involving the time-derivatives of the dipoles evaluated at retarded times. In the long distance approximation, the amplitude of dominant contribution only keeps a transverse component and becomes, at distance r from the source:

$$\boldsymbol{E}(\omega_3) = -\frac{\partial^2 D}{\partial t^2}\frac{\sin\theta_3^{[1]}}{rc^2}\boldsymbol{p}_{3+} = \frac{(\omega_3)^2}{rc^2}\boldsymbol{D}_T \tag{64}$$

We recover that, for emission at long distance, only the transverse component $\boldsymbol{D}_T$ of the dipole emits the electric field. When dipoles are uniformly distributed in a plane with surface density η, they create a surface polarization $\boldsymbol{P} = \eta\boldsymbol{D}$ and the total emitted field integrates the dipole elementary fields over the plane. This is in fact a classical calculation,[60] generalized to an arbitrary oriented $\boldsymbol{P}$. Integration over $2\pi r dr$ removes the proportionality to the inverse distance and retains only the normal wavevector dependence,[60] yielding an additional $2i\pi\eta/k_{3,z}^{[1]}$ factor which, coupled to Eq. 64, gives back Eq. 8. The form of the SFG field radiated from a plane interface is thus analogous to classical antenna emission spread over an infinitely thin plane.

It may be worried that SFG experiments miss some information because only the transverse component of the nonlinear polarization creates a measurable signal in the far field. As a matter of fact, the polarization is sometimes purely transverse (e.g. mixing s and p incoming polarization on an isotropic interface generates only s-polarized SFG) but often mixes both transverse and longitudinal components, and far field SFG intensity extracts no information from the longitudinal part indeed. Firstly, all the nonvanishing tensor components of $\chi^{(2)}$ participate to the transverse response, so they all contribute to the measured SFG signal. The ($\boldsymbol{x}$, $\boldsymbol{y}$, $\boldsymbol{z}$) frame nicely integrates the reflectivity effects through the Fresnel coefficients, but it also sticks to the symmetry elements of the interface.[61] Expressing tensor $\chi^{(2)}$ in this referential ensures that, for oblique incidences, all tensor components will appear in one of the eight polarization combinations expressed in terms of s and p for incident and SFG beams. Secondly, being experimentally limited to the transverse part of the nonlinear polarization makes it difficult to disentangle the various $\chi^{(2)}$ components from a single intensity measurement. This is well-known for example in the *ppp* polarization scheme

on an isotropic interface,[26] although incidence angle tuning[62,63] or polarization mapping[64] may help. We propose another way for this disentangling in Part V. Experimentally measuring the longitudinal polarization contribution would provide additional constraints and relationships between the $\chi^{(2)}$ components, and help their separation. Such a measurement requires to extract or enhance the near fields at the interface, because, contrary to Eq. 64, they mix both longitudinal and transverse polarization components. It has been shown for example how the coupling of the SFG process to the local excitation of surface plasmon resonances from nanoparticles modifies the selection rules for molecular hyperpolarizability components,[65] either in the functionnalized[66] or SHINE-SFG[65,67] geometries. In a different approach, longitudinal polarization components may also be probed by *in situ* near field measurement,[68,69] using for example an STM[70] or NSOM[71] tip to extract the signals.

4. Dispersion

Each individual Fresnel factor at an interface, related to one of the three beams, varies with the wavelength of light. Energy dispersion impacts on Fresnel factors through the indices of refraction and, consequently, the refracted angles. In the thin film model, the wavelength of light also tunes the interference term β_i. As SFG is essentially used as a spectroscopic tool, one must pay attention to the influence of Fresnel dispersion, which may distort the spectra. Spectral distortion has limited consequences and may be handled out when Fresnel dispersion remains featureless, only introducing a slope and a phase shift in the spectra. Still, this may cause some nuisance for accurate curve fitting and correct account of the nonresonant background. On the contrary, factors showing uneven dispersion and displaying marked maxima (or minima) introduce in experimental data a spectral modulation which may look like artifactual resonances or conversely mask actual resonant processes in the spectra.

The high energy beams of the SFG process (i.e. in the visible and near-infrared ranges) are sometimes experimentally tuneable or broadband, for example at two-colour (2C-)SFG[72,73] and electronic SFG set-ups.[23,74] When it is the case, the probed range is usually wide and the interfaces under study are designed to have strong resonant processes in the visible range, so the corresponding Fresnel factors are expected to vary when tuning the visible wavelength. Examples in the literature show that 2C-SFG users usually include Fresnel dispersion in

their data analysis, either when doubly resonant SFG processes,[23,75–80] electronic resonances at metal surfaces[46,47] or in nanostructures[66,81] are involved. Still, in the light of the examples below focusing on the infrared beam, one may consider that special care must be taken when one of the layers in the system consists of molecules with visible activity (e.g. chromophores) as a film with nonvanishing thickness (medium [2]) or as medium [3].

As for the infrared beam, Fresnel dispersion is usually less taken into account. This is not a problem when studying a molecular monolayer on a substrate, because the Fresnel factors in Eq. 58 do not depend on the monolayer properties, except for the squared refractive index of medium [2] in the z-factor. Even for an absorbing molecule, dispersion of this term remains limited and may be easily modeled. As shown in some examples,[12,13,82] problems occur for molecular layers involved as thin films (medium [2]) or semi-infinite bulks (medium [3]) if their molecular resonances in the infrared range (i.e. vibrations) are not correctly taken into account. This is due to the fact that, this time, the molecular optical properties fully take part in the Fresnel factors through reflection coefficients and $\beta(\omega_{IR})$. In addition, the molecular resonances at the origin of the linear Fresnel dispersion and nonlinear SFG resonances are the same. We briefly detail below the reasons underlying the peculiar behaviors of these systems, which are intrinsic to the Fresnel equations.

In Ref. 13, the authors show that "the Fresnel factor strongly influences the line shape of VSFG spectra when both the extinction coefficient of the detected species and the nonresonant amplitude in VSFG spectra are substantial". The system under study is the surface of propylene carbonate (PC), a molecular liquid, in the C=O stretching region. In order to quantify this effect, we model the complex dielectric function of the molecules by the sum of a constant real part $(\varepsilon^{[3]})_\infty$ and a complex Lorentzian correction as a function of the infrared wavenumber, supposed small with respect to the constant contribution. In the Supplementary Material, we show why, for a purely vibrationally resonant nonlinear susceptibility $\chi^{(2)}$, taking into account the linear resonant properties of the molecules only slightly distorts the measured SFG intensity. On the contrary, for a constant nonresonant $\chi^{(2)}$, the molecular Lorentzian resonance modulates the SFG intensity in the same way as it modulates the dielectric function. This gives the false impression that $\chi^{(2)}$ involves a resonant part, which amplitude may in addition be attributed an incorrect sign. In this first example, the behavior of the Fresnel factor is regular, i.e. it follows from the dispersion properties of the PC refractive index. As explained in the Supplementary Material, the dispersion of

$(\cos\theta^{[3]})^2$ in such a dispersive (Lorentzian) three-layer system is indeed regular, summing up a constant $[(\cos\theta^{[3]})^2]_\infty$ with a Lorentzian correction. On the contrary, the dispersion of $\cos\theta^{[3]}$ depends on the sign of $[(\cos\theta^{[3]})^2]_\infty$ and its amplitude with regard to the Lorentzian correction. For high positive $[(\cos\theta^{[3]})^2]_\infty$, $\cos\theta^{[3]}$ has a usual Lorentzian dispersion and we recover the simple conclusions recalled above for the air/PC interface. For high negative $[(\cos\theta^{[3]})^2]_\infty$, the IR beam experiences (or becomes close to) total internal reflection at the $\{13\}$ interface, whereas for low values of $[(\cos\theta^{[3]})^2]_\infty$ the situation is intermediate and becomes very sensitive to small changes to $[(\cos\theta^{[3]})^2]_\infty$. This is illustrated by the second example (sapphire/gold/water interface), studied in Ref. 12. The calculated dispersion of the F_x Fresnel factor has nothing to do with the refractive index of water, even if it is shown that the latter is the main source of Fresnel dispersion. In that example indeed, parameter $[(\cos\theta^{[3]})^2]_\infty$ remains small, and varies with the growing external angle of incidence from positive to negative values. This leads to dramatic changes in the dispersion lineshapes of $\cos\theta^{[3]}$ which, as shown in the Supplementary Material, account for the rather unpredictable shapes of the F_x factor.

In a broader perspective, these examples show how a dispersive refractive index in medium [3], even of molecular origin, may induce strong distortion of the Fresnel factors. In addition to the infrared, this identically applies to Fresnel factors in the visible range for systems involving chromophores, when the visible color is tuned. The situation is analogous, either for infrared or visible factors, in a dispersive medium [2] with a finite thickness, the critical parameter becoming $\cos\theta^{[2]}$ instead of $\cos\theta^{[3]}$. This case is in fact even more complex because $\cos\theta^{[2]}$ is involved in $r^{12}_{s/p}$, $r^{23}_{s/p}$ and β_i, making predictions rather impossible without a complete Fresnel analysis.

IV. INTERFERENCE AND CONTRAST: PRINCIPLES

Up to now, a single nonlinear sheet has been assumed, located at arbitrary depth z_0 inside the film in a two interface system. However, the thin film model is also useful when several nonlinear sources are considered, usually at depths $z_0 = 0$ and $z_0 = D$, because the interference patterns due to the different Fresnel coefficients modulate the experimental response of both interfaces.[7,11,15] We examine here the consequences of these interferences, with a focus on the conditions leading to the cancelling of the SFG signals produced at

one of the interfaces.[23] It is rather simple to analyze the oscillations of the electric field amplitude for one beam i inside the film from Eq. 24-26, giving rise to Airy profiles with period $\pi/\,\mathbb{R}\mathrm{e}(k_{i,z}^{[2]})$. The full SFG response, however, is modulated by the product of three of these Fresnel coefficients, and the general incommensurability of the three periods makes it impossible to draw universal conclusions on the dependence of the measured SFG signals as a function of z_0 or D, making the analysis of each specific situation necessary.[5,15,33]

When dealing with two SFG-active interfaces, one of the goals is to enhance the contrast, i.e. selectively probe one of them while keeping the other as silent as possible. From the equations above, it is indeed possible to establish the analytic laws concerning the selectivity of SFG spectroscopy on one of the two interfaces involved, to the detriment of the other, because the SFG process vanishes as soon as one of three fields involved in the frequency mixing cancels. In reflection, we may fruitfully compare the Fresnel activities at depths $z_0 = 0$ and $z_0 = D$ in order to understand in which conditions one of them overwhelms the other. Specifically, with the notations of Part III, we define the contrast ratios:

$$R_x = \frac{F_x^{film}(z_0 = 0)}{F_x^{film}(z_0 = D)} = \frac{1 - r_p^{23}(\omega_i)e^{2i\beta_i}}{[1 - r_p^{23}(\omega_i)]e^{i\beta_i}} \tag{65}$$

$$R_y = \frac{F_y^{film}(z_0 = 0)}{F_y^{film}(z_0 = D)} = \frac{1 + r_s^{23}(\omega_i)e^{2i\beta_i}}{[1 + r_s^{23}(\omega_i)]e^{i\beta_i}} \tag{66}$$

$$R_z = \frac{F_z^{film}(z_0 = 0)}{F_z^{film}(z_0 = D)} = \frac{1 + r_p^{23}(\omega_i)e^{2i\beta_i}}{[1 + r_p^{23}(\omega_i)]e^{i\beta_i}} \tag{67}$$

Enhancing the contrast in favor of interface $z_0 = 0$ requires to minimize, or cancel, the Fresnel factor at $z_0 = D$. We remind that $1 \pm r_{s/p}^{23} = 0$ is usually not achieved, especially with usual dielectrics, because it would require one of the conditions $n^{[2]}$, $n^{[3]} = 0$ or $\theta^{[2]}$, $\theta^{[3]} = 90°$. The first condition is never fulfilled in usual materials[83] and the second one only for total internal reflection (TIR) at the critical angle.[56] The electric field amplitudes at $z_0 = D$ therefore do not exactly vanish, but one may still reduce them to favour the $z_0 = 0$ interface by bringing the values of $r_{s/p}$ close to ± 1. This is done by working at angles of incidence $\theta^{[1]}$ close to 90°, as has been checked experimentally.[15] Other possibilities include working close to critical TIR angle or designing $|n^{[2]}| \gg$ (or $\ll$) $|n^{[3]}|$, for example at a dielectric-metal interface, in particular in the infrared. These conditions do not depend on thickness D, which, together with the angles of incidence (and for some respect the wavelengths), is the parameter that one would like to use to modulate the contrast. Another possibility, for

an absorbing medium [2], is to increase thickness D until $e^{i\beta_i}$ becomes so small, through $e^{-\mathbb{Im}(\beta_i)}$, that no field reaches interface $z_0 = D$, but this makes the design of the three-layer system pointless as it reduces the Fresnel factors to those of a simple two-layer system.

Enhancing the contrast in favor of interface $z_0 = D$, i.e. minimizing $|R_{x/y/z}|$, is in fact more interesting because it allows to extract the SFG response of the buried interface with no, or little, perturbation from the first interface. The amplitudes of the ratios $R_{x/y/z}$ above depend on D, essentially through the Fresnel factor at $z_0 = 0$. It is therefore conceivable to minimize the contribution from that interface by an appropriate choice of D, linked to the values of the angle of incidence $\theta_i^{[1]}$ and the indices of refraction of the three media. A complete analysis of this minimization problem is given in the Appendix, for generic values of indices $n^{[2]}$ and $n^{[3]}$ in the complex plane. It shows that it is possible to find periodic minima for the Fresnel factors at $z_0 = 0$ (or for the contrast ratios) as a function of D as long as the magnitude of the reflection coefficient $|r_{s/p}^{23}|$ is not too far from 1 and absorption in medium [2] not too prohibitive. The first condition is usually difficult to fulfill in transparent, low absorbing dielectrics because the indices in media [2] and [3] remain close to each other. However, involvement of total internal reflection (TIR) configuration, or of media with a high absorption coefficient (i.e. high imaginary part of the refractive index), makes it possible to determine ranges of thicknesses leading to minimizing one of the Fresnel factor at $z_0 = 0$, hence the SFG process at this interface. Other non-periodic (i.e. single) minima occur, for p-polarization only, provided that, paradoxically, absorption strongly dominates over propagation in media [2] and [3].

Here below we focus more precisely on the conditions on thickness D leading to the exact cancellation of one of the contrast ratios above. In these situations, the SFG experimental signals solely originate from the $z_0 = D$ layer. Experimentally, D value can be adjusted to favor this exact cancellation, or approximate it, at one or several angles of incidence. Of course, when the exact conditions below are not strictly, but only approximately, fulfilled (either because the experimental D does not correspond to the predicted one or because the refractive indices are not perfectly real or imaginary), the corresponding Fresnel factor still shows a marked minimum and a clear contrast between the two interfaces is expected.

The conditions, depending on D, are: $r_p^{23}(\omega_i) = e^{-2i\beta_i}$ for x, $r_s^{23}(\omega_i) = -e^{-2i\beta_i}$ for y and

$r_p^{23}(\omega_i) = -e^{-2i\beta_i}$ for z. From the expressions of $r_{s/p}^{23}$ in Eq. 4 and 5, this leads for beam i to:

$$\tan\beta_i = \frac{n_i^{[2]}\cos\theta_i^{[3]}}{i\,n_i^{[3]}\cos\theta_i^{[2]}} \text{ for } x \tag{68}$$

$$\tan\beta_i = \frac{n_i^{[2]}\cos\theta_i^{[2]}}{i\,n_i^{[3]}\cos\theta_i^{[3]}} \text{ for } y \tag{69}$$

$$\tan\beta_i = \frac{n_i^{[3]}\cos\theta_i^{[2]}}{i\,n_i^{[2]}\cos\theta_i^{[3]}} \text{ for } z \tag{70}$$

The results in the Appendix show that exact vanishing of Eq. 65-67 is only possible when the refractive indices in media [2] and [3] are either purely real or imaginary, which restrains the possible scenarios. In order to fulfill equalities in Eq. 68-70, at least one of the quantities $n_i^{[2]}\cos\theta_i^{[2]}$ and $n_i^{[3]}\cos\theta_i^{[3]}$ must be an imaginary number. Inserting $\beta_i = \frac{\omega_i D}{c} n_i^{[2]}\cos\theta_i^{[2]}$, it is easy to show by examination of the various possibilities that $n_i^{[3]}\cos\theta_i^{[3]}$ is in fact always imaginary, as was also determined in the Appendix. There are two ways to achieve this: (i) in the total internal reflection (TIR) regime at the $\{23\}$ interface ($\cos\theta^{[3]}$ is imaginary) and (ii) for imaginary refractive index $n^{[3]}$. Condition (ii) is fulfilled for example for a perfect free electron metal below the interband transition threshold, in the wavelength regime where damping may be neglected, leading to $\mathbb{R}\mathrm{e}(n^{[3]}) \ll \mathbb{I}\mathrm{m}(n^{[3]})$. This is fairly the case in the visible and near-infrared ranges for Ag, Au (threshold ∼600nm), Cu (∼650nm), Pt (∼500nm), and for some other transition metals in the infrared only. This means that field cancellation at $z_0 = 0$ cannot happen when layer 3 is a dielectric medium in which the beam freely propagates (i.e. no TIR).[15]

We may have a closer look at each situation:

- (i)-a: TIR propagation in medium [3], not in medium [2]. We recall that TIR at the $\{23\}$ interface happens when $\sin\theta_i^{[3]}$ becomes bigger than 1. We have $n_i^{[2]}$, $n_i^{[3]}$, $\cos\theta_i^{[2]}$ and β_i real and positive, whereas $\cos\theta_i^{[3]} = i\sqrt{\sin^2\theta_i^{[3]} - 1}$ with $\theta_i^{[1]}$ bigger than the TIR critical angle for the $\{13\}$ interface. For given values of the angle of incidence and of the refractive indices in media [2] and [3], the periodicity of the tangent function implies that several values D_i lead to the cancellation of the Fresnel factor at the $z_0 = 0$ interface, following a periodic series with period $T(\omega_i) = \dfrac{\lambda_i}{2n_i^{[2]}\cos\theta_i^{[2]}}$ independent on the polarization, namely, for $k \geqslant 0$:

$$D_{i,x} = \frac{\lambda_i}{2\pi n_i^{[2]}\cos\theta_i^{[2]}}\left[\arctan\left(\frac{n_i^{[2]}\sqrt{\sin^2\theta_i^{[3]} - 1}}{n_i^{[3]}\cos\theta_i^{[2]}}\right) + k\pi\right] \text{ for } x \tag{71}$$

$$D_{i,y} = \frac{\lambda_i}{2\pi n_i^{[2]} \cos\theta_i^{[2]}} \left[\arctan\left(\frac{n_i^{[3]} \sqrt{\sin^2\theta_i^{[3]} - 1}}{n_i^{[2]} \cos\theta_i^{[2]}} \right) + \frac{\pi}{2} + k\pi \right] \text{ for } y \qquad (72)$$

$$D_{i,z} = \frac{\lambda_i}{2\pi n_i^{[2]} \cos\theta_i^{[2]}} \left[\arctan\left(\frac{n_i^{[2]} \sqrt{\sin^2\theta_i^{[3]} - 1}}{n_i^{[3]} \cos\theta_i^{[2]}} \right) + \frac{\pi}{2} + k\pi \right] \text{ for } z \qquad (73)$$

where we have used $\arctan x + \arctan(1/x) = \mathrm{sgn}(x)\frac{\pi}{2}$. We note that the cancellation thicknesses are proportional to the wavelength of light λ_i and differ for the three orientations of the electric fields. The first $D_{i,x}$ lies between 0 and $\frac{\lambda_i}{4n_i^{[2]}\cos\theta_i^{[2]}}$ ($\tan\beta_i > 0$), whereas the first $D_{i,y}$ and $D_{i,z}$ lie between $\frac{\lambda_i}{4n_i^{[2]}\cos\theta_i^{[2]}}$ and $\frac{\lambda_i}{2n_i^{[2]}\cos\theta_i^{[2]}}$ ($\tan\beta_i < 0$). As $D_{i,z} - D_{i,x} = T(\omega_i)/2$, there is also no cancellation thickness common to x and z components involved in p-polarization. Finally, as media [2] and [3] are dielectric, their refractive indices are not too far apart and thicknesses $D_{i,y}$ and $D_{i,z}$ have nearby values.

- (i)-b: TIR propagation in medium [3] and in medium [2]. We have $n^{[2]}$, $n^{[3]}$ real and positive, whereas $\cos\theta_i^{[2]} = i\sqrt{\sin^2\theta_i^{[2]} - 1}$ and $\cos\theta_i^{[3]} = i\sqrt{\sin^2\theta_i^{[3]} - 1}$. β_i is a positive imaginary number for positive D, and so is $\tan\beta_i$. However, from Eq. 68-70, $\tan\beta_i$ has to be a negative imaginary number and, consequently, there is no positive thickness making these equalities possible: the Fresnel factors at the $\{12\}$ interface cannot vanish whatever the thickness D. In this case, we have indeed $|r_{s,p}^{23}| < 1$.

- (i)-c: TIR propagation in medium [3], imaginary index in medium [2]. Here medium [2] is for example a free electron metal, and $n_i^{[2]} = i\kappa_i^{[2]}$ with $\kappa_i^{[2]} > 0$, $n_i^{[3]}$ and $\cos\theta_i^{[2]} > 1$ are real and positive, whereas $\cos\theta_i^{[3]} = i\sqrt{\sin^2\theta_i^{[3]} - 1}$. β_i is a positive imaginary number and we have $\tan\beta_i = i\tanh\left(\frac{\omega_i\kappa_i^{[2]}\cos\theta_i^{[2]}}{c}D\right)$. There is no solution for y component to Eq. 69, as its right hand side is a negative imaginary number (we have $|r_s^{23}| < 1$). Considering x- and z-polarizations, there is a single thickness D leading to cancellation of the field for only one of them, depending whether $\frac{n_i^{[3]}\cos\theta_i^{[2]}}{\kappa_i^{[2]}\sqrt{\sin^2\theta_i^{[3]} - 1}}$ is smaller (cancellation for z component) or bigger (cancellation for x component) than

unity. For example, in the former case, we find:

$$D_{i,z} = \frac{\lambda_i}{2\pi\kappa_i^{[2]}\cos\theta_i^{[2]}}\,\mathrm{artanh}\left(\frac{n_i^{[3]}\cos\theta_i^{[2]}}{\kappa_i^{[2]}\sqrt{\sin^2\theta_i^{[3]}-1}}\right) \tag{74}$$

Of course here, additional effects come into play: amplitudes of the electric fields in medium [2] decrease as a function of thickness D as a consequence of strong absorption on the path, and may become negligible at the $\{23\}$ interface if D is bigger than the skin depth. The analysis of the Appendix explains why this should not be an issue. The absolute values of the Fresnel factors at both interfaces also have to be monitored (and not only their ratios) because they may become small for some coordinate as a consequence of the optical properties of metals (i.e. $r_s^{12} \approx -1$, $r_p^{12} \approx 1$ and $r_p^{23} \approx -1$ at the dielectric metal interfaces).

- (ii)-a: imaginary index in medium [3], normal propagation in medium [2]. Here there is no TIR at any interface, and we have $n_i^{[2]}$, $\cos\theta_i^{[2]}$ and β_i real and positive, whereas $n_i^{[3]} = i\kappa_i^{[3]}$ with $\kappa_i^{[3]} > 0$, leading to $\cos\theta_i^{[3]} > 1$ and real. Solving Eq. 68-70 shows that it is possible to cancel the electric field at interface $z_0 = 0$ for a series of thicknesses with the same period as in (i)-a, and defined for $k \geqslant 0$ as:

$$D_{i,x} = \frac{\lambda_i}{2\pi n_i^{[2]}\cos\theta_i^{[2]}}\left[\arctan\left(\frac{\kappa_i^{[3]}\cos\theta_i^{[2]}}{n_i^{[2]}\cos\theta_i^{[3]}}\right)+\frac{\pi}{2}+k\pi\right] \text{ for } x \tag{75}$$

$$D_{i,y} = \frac{\lambda_i}{2\pi n_i^{[2]}\cos\theta_i^{[2]}}\left[\arctan\left(\frac{\kappa_i^{[3]}\cos\theta_i^{[3]}}{n_i^{[2]}\cos\theta_i^{[2]}}\right)+\frac{\pi}{2}+k\pi\right] \text{ for } y \tag{76}$$

$$D_{i,z} = \frac{\lambda_i}{2\pi n_i^{[2]}\cos\theta_i^{[2]}}\left[\arctan\left(\frac{\kappa_i^{[3]}\cos\theta_i^{[2]}}{n_i^{[2]}\cos\theta_i^{[3]}}\right)+k\pi\right] \text{ for } z \tag{77}$$

We recover as above the half-period difference between $D_{i,x}$ and $D_{i,z}$, and the predictable close values between $D_{i,x}$ and $D_{i,y}$.

- (ii)-b: imaginary index in medium [3], TIR propagation in medium [2]. We have $n_i^{[2]}$ and $\cos\theta_i^{[3]} > 1$ real and positive, whereas $\cos\theta_i^{[2]} = i\sqrt{\sin^2\theta_i^{[2]}-1}$ and $n_i^{[3]} = i\kappa_i^{[3]}$ with $\kappa_i^{[3]} > 0$. β_i is a positive imaginary number for positive D, and so is $\tan\beta_i$. From Eq. 68-70, we deduce, as in case (i)-c, that there is no positive thickness D to fulfil Eq. 69 (y-polarization), and that there is a single one leading to the cancellation of

either the x- or z-component of the electric field, depending on the relative values between $\frac{\kappa_i^{[3]}\sqrt{\sin^2\theta_i^{[2]}-1}}{n_i^{[2]}\cos\theta_i^{[3]}}$ and 1. For example, z-component cancels for

$$D_{i,z} = \frac{\lambda_i}{2\pi n_i^{[2]}\sqrt{\sin^2\theta_i^{[2]}-1}}\,\mathrm{artanh}\left(\frac{\kappa_i^{[3]}\sqrt{\sin^2\theta_i^{[2]}-1}}{n_i^{[2]}\cos\theta_i^{[3]}}\right) \tag{78}$$

when the ratio is smaller than 1. Here, it is in addition required that thickness D remains small enough to allow the evanescent wave crossing medium [2] to reach interface {23} without excessive amplitude damping, which should be the case for the values calculated here.

- (ii)-c: imaginary index in media [3] and [2]. With $n_i^{[2]} = i\kappa_i^{[2]}$ and $n_i^{[3]} = i\kappa_i^{[3]}$, β_i is a positive imaginary number for positive D, and so is $\tan\beta_i$. From Eq. 68-70, $\tan\beta_i$ has to be a negative imaginary number and, consequently, there is, as in case (i)-b, no positive thickness D fulfilling these equalities. Accordingly, we may check that $|r_{s,p}^{23}| < 1$.

As a conclusion, for the ideal situations listed above and summarized in Table I, it is possible to define the relationship between thickness D and angle of incidence $\theta^{[1]}$ leading to the cancellation of one electric field at the $z_0 = 0$ interface, as a result of interferences between reflected beams oscillating in medium [2]. These results remain a fair approximation when the dielectric indices have a small imaginary part, or the imaginary indices a small real part, leading to the observation of a minimum, instead of an exact cancellation, in the Fresnel factors (and field amplitudes) in actual experiments. The minima in this case are found using Eq. A2, A6 and A7 instead of Eq. 71-78. Still, the existence and predictability of such accurate cancellation (or minimum) conditions does not exempt to compute the three Fresnel factors for the full SFG process using the calculated parameters, in order to check that SFG shall indeed be produced and measured at interface $z_0 = D$.

When SFG is measured in transmission, the conditions change (for beam 3 only) as the role of media [1] and [3] are switched. The cancellation conditions follow from Eq. 48-53:

$$\frac{F_x^{film,T}(z_0=D)}{F_x^{film,T}(z_0=0)} = \frac{1-r_p^{21}(\omega_3)e^{2i\beta_3}}{[1-r_p^{21}(\omega_3)]e^{i\beta_3}} \tag{79}$$

$$\frac{F_y^{film,T}(z_0=D)}{F_y^{film,T}(z_0=0)} = \frac{1+r_s^{21}(\omega_3)e^{2i\beta_3}}{[1+r_s^{21}(\omega_3)]e^{i\beta_3}} \tag{80}$$

Case	Medium 2	Medium 3	Scheme	Cancellation (thickness D)
(i) - a	Propagative dielectric	TIR in dielectric	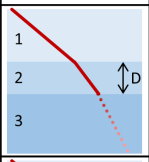	Periodic Eq. (71)-(73)
(i) - c	Imaginary index (free electron metal)	TIR in dielectric	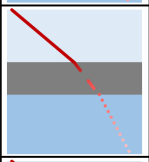	Single Eq. (74)
(ii) - a	Propagative dielectric	Imaginary index (free electron metal)	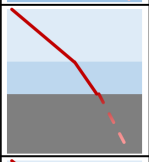	Periodic Eq. (75)-(77)
(ii) - b	TIR in dielectric	Imaginary index (free electron metal)	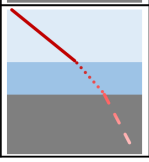	Single Eq. (78)

TABLE I. Properties of the three-layer systems where cancellation of a Fresnel factor at interface $z_0 = 0$ may occur. Plain lines represent propagating light waves, dashed lines light waves in a metal (grey color), dotted lines TIR waves in a dielectric (blue color).

$$\frac{F_z^{film,T}(z_0 = D)}{F_z^{film,T}(z_0 = 0)} = \frac{1 + r_p^{21}(\omega_3)e^{2i\beta_3}}{[1 + r_p^{21}(\omega_3)]e^{i\beta_3}} \tag{81}$$

and, this time, the electric field for beam 3 may be cancelled at interface $z_0 = D$ under the conditions, symmetric to Eq. 68-70:

$$\tan\beta_3 = \frac{n^{[2]}\cos\theta^{[1]}}{i\,n^{[1]}\cos\theta^{[2]}} \text{ for } x \tag{82}$$

$$\tan\beta_3 = \frac{n^{[2]}\cos\theta^{[2]}}{i\,n^{[1]}\cos\theta^{[1]}} \text{ for } y \tag{83}$$

$$\tan\beta_3 = \frac{n^{[1]}\cos\theta^{[2]}}{i\,n^{[2]}\cos\theta^{[1]}} \text{ for } z \tag{84}$$

The same analysis as above may be performed, and optimal thicknesses leading to field cancellations at the $z_0 = D$ interface for the SFG beam may be found in case (i), i.e. when total reflection occurs at the $\{21\}$ interface. Such a TIR configuration is compatible indeed with the propagation of the incoming beams at the $\{12\}$ interface. In IR-visible SFG experiments, considering that the angles of incidence for the visible ($\theta_1^{[1]}$) and SFG ($\theta_3^{[1]}$) beams are in general close to each other, whereas IR angle $\theta_2^{[1]}$ is free, a particular

attention is required if mixing cancelling conditions for the incoming beams at $z_0 = 0$ and for transmitted SFG beam at $z_0 = D$ is intended (e.g. counter-propagative geometry). On the contrary, case (ii) cannot be applied to the SFG beam in transmission because it would suppose that medium [1] is semi-infinite and metallic, which is not suitable for the propagation of the incident beams.

V. EXAMPLES OF HIGH CONTRAST SYSTEMS

We illustrate here the laws elaborated above and in the Appendix by calculating contrast ratios (for the field intensities, that is $|R_{x/y/z}|^2$) in various systems, leading to experimental applications using specific configurations. In the following examples, interfaces involve polymer layers because their thicknesses are easily adjusted during sample preparation. Still, any dielectric, including for example liquid water or low absorbing solids, may replace the polymer and lead to the same results as long as their refractive indices fall into the same ranges.

1. Dielectric/polymer/air and dielectric/polymer/water systems

In the first example, we use the system studied in Ref. 15 and composed of a hemicylindrical fused silica prism, a PDMS polymer layer of variable thickness D, and a dielectric medium [3] chosen here as air or water. It is representative of a class of systems consisting of a high index transparent dielectric material, an intermediate and mostly transparent layer, and a low index material (transparent or not). All refractive indices are taken identical to the original publication, visible wavelength is 532nm and infrared wavenumber in the middle of the experimental range (2925cm^{-1}). In order to easily locate the minima of the contrast ratios as a function of the incident angle $\theta_i^{[1]}$ and D, we plot the intensities of the inverse contrast ratios in 2D maps in Fig. 2. For air as medium [3], the series of periodic minima for the visible beam appear as maxima in Fig. 2(A) for x and y components, and in (B) for z component (with both interfaces belonging to medium [2]), showing values close to y. As all refractive indices are real, there is no attenuation as D increases for a fixed angle. This can be checked on the insert graph in panel (A) displaying the evolution of the intensity of the contrast ratios, extracted as a function of D for $\theta_1^{[1]} = 50°$. Analogous curves for the

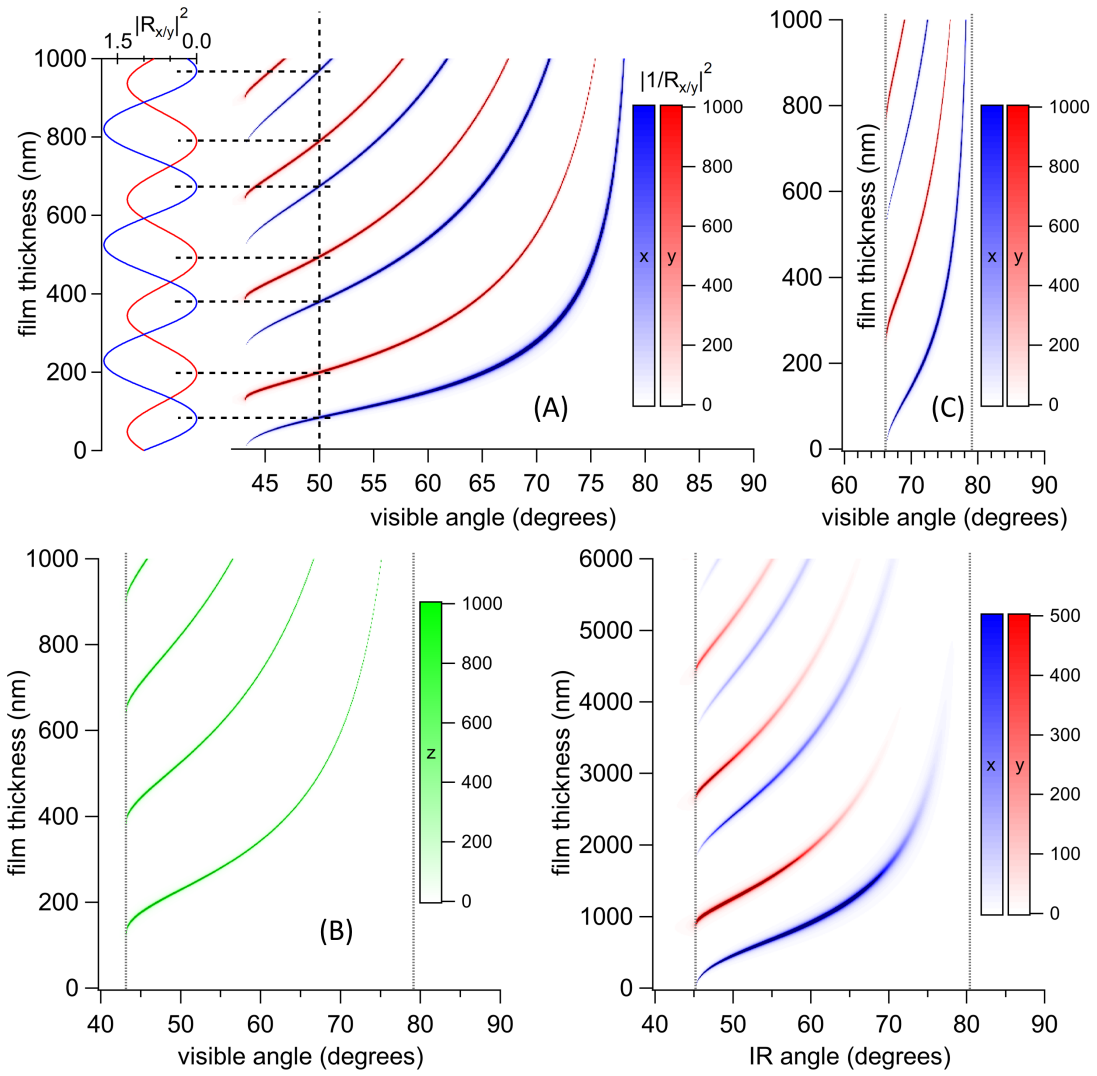

FIG. 2. Contrast factors at the silica/PDMS/air and silica/PDMS/water systems. (A) 2D plot of $|1/R_x|^2$ (blue) and $|1/R_y|^2$ (red) for air at 532nm as a function of film thickness D and visible angle of incidence in silica. Insert shows $|R_x|^2$ and $|R_y|^2$ at incidence 50°. (B) Same as (A) for $|1/R_z|^2$ (green), with z factors evaluated in medium [2]. (C) Same as (A) for water as the last medium. (D) Same as (A) for the infrared beam. Visible wavelength: 532nm, IR wavenumber: 2925cm^{-1}. Dotted lines indicate the critical angles for total internal reflection at the {silica/PDMS} and {PDMS/air} (resp. {PDMS/water}) interfaces.

SFG beam exhibit a slightly lower period. When the inverse intensity ratios for the infrared beam are considered (Fig. 2D), the larger period is observed, and the small imaginary part of the PDMS refractive index induces a gradual fading of the minima due to absorption during the journey through medium [2]. When medium [3] is taken as water, the behaviour

is the same but the allowed range for the incident angle is reduced. As a matter of fact, we visualize here the periodic minima in case (i)-a, which supposes a TIR configuration at the {PDMS/air} (resp. {PDMS/water}) interface, and no TIR at the {silica/PDMS} interface. The available range of incidence angles is therefore sandwiched between the critical angles of the two interfaces, as marked by the dashed lines in panels (B), (C) and (D). When air is replaced by water, the critical angle at 532nm for the {PDMS/water} interface raises in silica from 43.2 to 66.3°. The results in Fig. 2 match and extend those presented in Ref. 15. Finally, we note that x-component may cancel even for very small values of the film thickness close to the critical angle. One should however avoid working too close to this angle as it will also lead to the cancellation of the x Fresnel factor at interface $z_0 = D$.

Considering that the contrast ratios in Fig. 2 reach values better than 10^5:1 in the visible, and 10000:1 in the IR, these data allow to design an experiment in terms of D and $\theta^{[1]}$ in order to achieve cancellation of a given component of one of the three electric fields at the $z_0 = 0$ interface. In practice, when the component is y and isotropy in the film is assumed, nonlinear susceptibility components yyz, yzy and zyy (hence polarization combinations ssp, sps and pss) can all together be made specific of the buried interface $z_0 = D$. This may be achieved for a fixed thickness (i.e. a single sample) by adjusting two of the three angles of incidence, or by designing several films with a variable D using fixed experimental angles of incidence (assuming that the interfacial response, e.g. molecular orientation or composition, does not change with D). Such an evolution of SFG amplitudes as a function of thickness and angles of incidence has already been experimentally evidenced[84] together with interface selectivity,[15,24] sometimes relying on empirical rules.[85,86] Still it must be checked that, in the conditions chosen, the Fresnel factor at interface $z_0 = D$ does not become too small (as a consequence of absorption in medium [2] or because $r^{23}_{s/p}$ is too close to ± 1) in order to be able to measure the SFG signal from that interface. Combination ppp is more challenging because it involves four components (xxz, xzx, zxx and zzz), so cancelling one of the fields at $z_0 = 0$ still leaves two components active. We have also seen previously that the thicknesses leading to cancellation for x and z were distinct by half a period, so it is not possible to cancel both x and z for the same beam. However, we see on Fig. 2 (A), (B) and (D) that the curves describing the minima for the infrared and visible beams intersect for particular values of the (D, $\theta^{[1]}$) couples, and accordingly for the SFG and IR beams.

In Fig. 3, we superimpose the minima for the visible and SFG beams (up to sixth order)

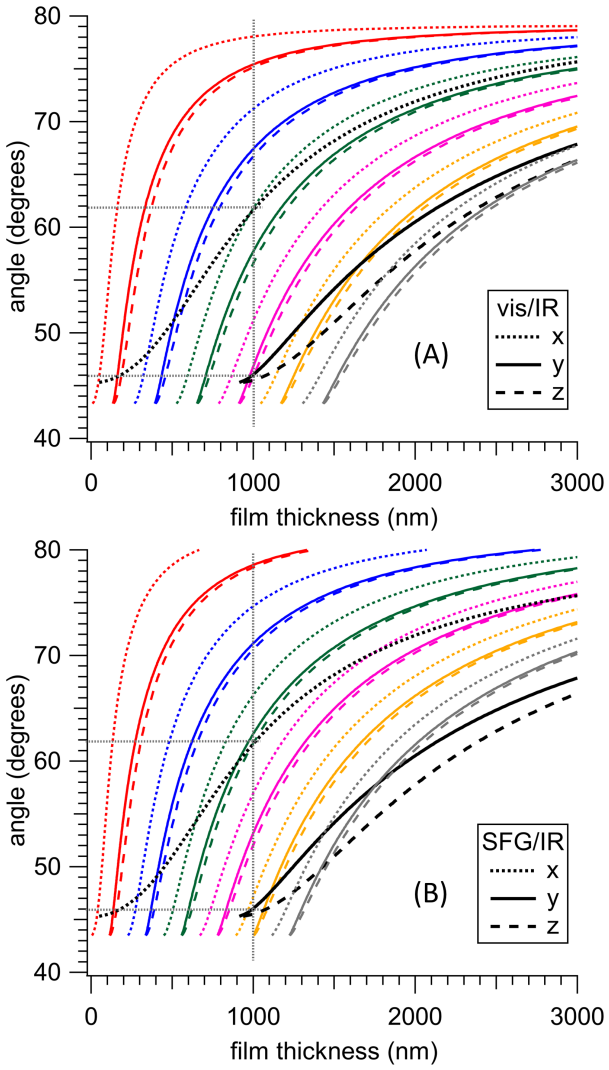

FIG. 3. Location of the minima of the contrast ratios $|R_x|$, $|R_y|$ and $|R_z|$ for the silica/PDMS/air system as a function of film thickness and angle of incidence in silica (A) for the visible and IR beams; (B) for the SFG and IR beams. Each color represents an order of the periodic minima for the visible and SFG beams, from 1 to 6. Only first order minima are shown in black for the IR.

to those of the IR beam (at first order), calculated using Eq. 71-73. These serve as an abacus to design favourable experimental settings, showing that it possible to cancel several components of the electric fields at $z_0 = 0$ at the same time. For example, with a 1000nm film, setting IR and visible incidences around 62° and 46° allows to cancel x-component of the IR at the first interface, together with y or z-component of the visible. When interchanging the values of the incidences, the cancelled components are swapped. In the first case, only xxz combination remains in a *ppp* experiment, and xzx in the second case. The same angles

applied to the IR and SFG beams lead to the cancellation of the same components for both beams, leading to the selection of zzz and xzx, respectively. Of course, accurate angle values must be determined from the curves and implemented. As for the IR, it is advisable to plot the abacus for a wavenumber corresponding to the frequency of the vibration mode under study. Alternatively, when experimental angles of incidence cannot be tuned at will, several crossing points can still be probed by designing several films with different thicknesses. The total *ppp* SFG response therefore sums up the full *ppp* from $z_0 = D$ interface interfering with only one of the four components of the $z_0 = 0$ interface. Such a configuration may give experimental access to the individual xxz, xzx, zxx and zzz components at the first interface as long as the interference is properly modelled, helping disentangle the *ppp* response. This thick film configuration is often considered because it allows to suppress the response from the first interface and measure only that of the buried interface. However, if an SFG-active molecular monolayer is placed at the first interface, but none at the second interface, the measured *ppp* SFG response is this time directly produced by only one of the four nonlinear susceptibility components at $z_0 = 0$, giving this time straightforward access to the experimental breaking up of the *ppp* response into its four components. It is known for example that polarization measurements give access to information about molecular orientation, but this often involves molecular modelling to disentangle the four components from the *ppp* response.[54,87]

2. Air/polymer/metal systems

In line with the previous example, we may turn to case (ii)-a by replacing medium [3] with a free electron metal. This time, no TIR configuration is needed so medium [1] may be simply chosen as air, and the polymer in medium [2] represents a large class of mostly transparent materials. An example of contrast variation with film thickness may be found in the air/PMMA/Ag system.[20] When air is replaced by fused silica and thickness varied,[21] contrast minima are still present whereas Fresnel contribution at the buried interface is constant as a consequence of index matching between silica and PMMA, leading to $r^{12}_{s/p} \approx 0$. Fig. 4 shows the inverse contrast ratios for the visible beam (532nm) for y and z components (x values being close to y values) in the air/PDMS/Ag and air/PDMS/Au systems. Optical constants of the metals are taken from Ref. 88 and 89. The optical properties of both metals

differ: silver is a nearly perfect free electron metal in the visible, which index of refraction is close to a pure imaginary number. On the contrary, gold at this wavelength exhibits a strong interband contribution, leading to an additional real part for its refractive index. For both metals, a series of periodic minima at $z_0 = 0$ are observed as a function of film thickness at all angles of incidence, making the design of experimental applications more simple than in the previous case. The main differences lies in the depths of the minima, reaching almost exactly zero for silver (contrast ratios up to 5000:1 for y and 25000:1 for z) but not for gold, especially at high angles of incidence (maximal contrast is around 100:1 for z and 45:1 for y). Still an interesting contrast between $z_0 = 0$ and $z_0 = D$ may be reached in the gold case at most angles. For z-component, the first minimum is accessible for small film thickness, far below the wavelength, still with a high contrast: at 50° incidence, a 76nm thick film produces a contrast better than 15000:1 in intensity for silver and, for gold, contrast reaches 62:1 for a 64nm film. We note that a much better contrast for gold (of the same order of magnitude as for silver) can be achieved for light with frequencies outside the interband domain, that is for wavelengths above 600nm, including in particular the infrared range. Contrary to the previous case, the curves gathering the minima in the IR and visible ranges do not cross (Fig. 4C and D). However, it still remains possible, by choosing a single film thickness, to cancel at the same time several components of two of the three beams by independently playing with the visible and IR angles of incidence. The conclusions drawn in the previous case therefore remain valid.

3. Dielectric/polymer/metal systems

The previous system may be modified to introduce a high index dielectric material as medium [1]. We follow Ref. 12 and choose sapphire (hence designing sapphire/PDMS/metal systems) for its transparency in a broad infrared range. Other high refractive index, IR-transparent materials include for example zinc sulfide, zinc selenide and diamond.[13] The 2D plots of the inverse contrast ratios $|1/R_x|^2$ and $|1/R_z|^2$ are displayed in Fig. 5 for a visible beam at 532nm (A-B) and 800nm (C-D), and for the IR at 3300cm^{-1} (E-F), with silver and gold as metals. We recover the periodic minima as expected on the low angle region of the graphs (with values for y close to those for x-component). In this region, all conclusions drawn in the previous systems remain valid, with maximal ratios for silver varying between

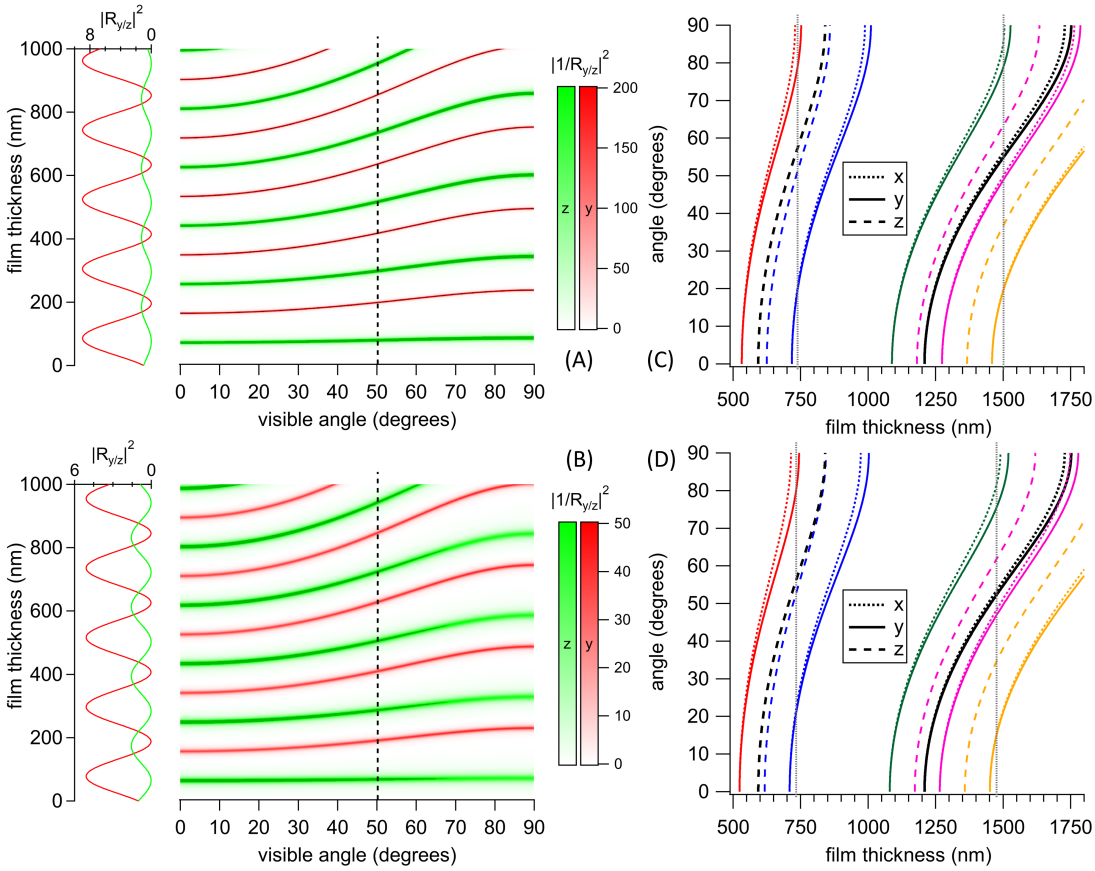

FIG. 4. Left: contrast factors at the air/PDMS/metal systems at 532nm. 2D plot of $|1/R_y|^2$ (red) and $|1/R_z|^2$ (green) (A) for silver and (B) for gold as a function of film thickness D and visible angle of incidence in silica (z factors evaluated in medium [2]). Inserts show $|R_y|^2$ and $|R_z|^2$ at incidence 50°. Darker zones indicate numbers above the highest values of the color scales. Right: location of the minima of the contrast ratios $|R_x|$, $|R_y|$ and $|R_z|$ for the air/PDMS/metal system as a function of film thickness and angle of incidence in silica for the visible and IR beams (C) for silver and (D) for gold. Each color represents an order of the periodic visible minima (from 3 to 8), only curves sharing a common film thickness with the IR curve (order 1, black) are shown.

10^4:1 and 10^5:1, except for x in the IR with a maximum at 600:1. For gold, the ratios peak at 700:1 and 100:1 at 532nm for x and z, respectively; 3500:1 and 18000:1 at 800nm; 300:1 and 70000:1 in the IR. As in the silica/PDMS/air system, the periodic minima disappear above the TIR critical angle of the {sapphire/PDMS} interface, marked by the dotted lines. However this time, other kinds of minima appear above this threshold. Looking first at the infrared range, the x-component at $z_0 = 0$ cancels out for very small thicknesses at high

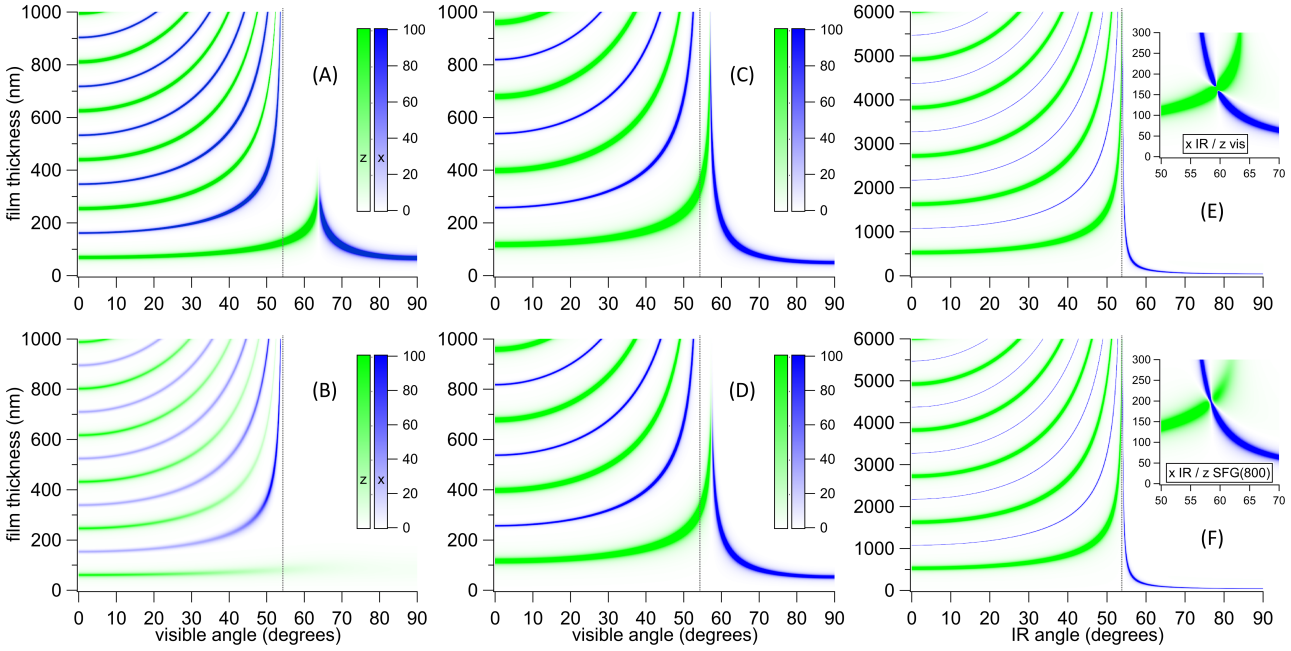

FIG. 5. Contrast factors at the sapphire/PDMS/metal systems. 2D plot of $|1/R_x|^2$ (blue) and $|1/R_z|^2$ (green) for silver (A, C, E) and for gold (B, D, F) as a function of film thickness and visible angle of incidence in sapphire (z factors evaluated in medium [2]). Visible wavelengths are 532nm (A-B) and 800nm (C-D), IR wavenumber is 3300cm^{-1} (E-F). Insets show the $|1/R_x|^2$ ratio in the IR with $|1/R_z|^2$ (E) at 532nm and (F) at the SFG wavelength for a visible at 800nm. Dotted lines indicate the critical angle for total internal reflection at the sapphire/PDMS interface. All color scales are equal.

angles. This is accounted for by the fact that, when crossing the TIR threshold, we switch from case (ii)-a to another regime described by case (ii)-b, characterized by the existence of a single minimum for either x or z. As explained in the Appendix, the mere existence of this non periodic minimum for low values of D guarantees that absorption through medium [2] does not hamper SFG production at $z_0 = D$ interface. In the infrared, the imaginary parts of the refractive indices of both metals in the infrared are very high, accounting for the selection of x component as explained in point (ii)-b. When turning to the visible range, the refractive indices of the metals decrease. At critical angle, the ratio in Eq. 78 vanishes, then increases with $\theta^{[1]}$. Minima thus first relate to the z-component close to the critical angle. Then, with a high refractive index material in medium [3], the increasing ratio exceeds 1 with growing angle and the minimum switches to x in the high angle region, as observed

in panels (A), (C) and (D) which pertain to almost perfect free electron metal. For gold in the green region (Fig. 5B), the influence of interband contribution is obvious as periodic minima become less intense. In the non periodic zone, propagation linked to the real part of the refractive index of gold becomes so strong that the minima fade with growing angle. For example, maximum contrast $|R_z|^2$ at $\theta^{[1]}$=60° and D = 64nm reaches only 12.4:1, to compare to the value of 75:1 at $\theta^{[1]}$=20° for D = 63nm.

As above, experimental conditions may be designed in the periodic regime to cancel out the contribution from $z_0 = 0$ interface, or some nonlinear susceptibility components in the *ppp* response at that interface. In the non periodic regime, the swapping between x and z-components also generates a crossing point between the minima in the visible and infrared ranges. As illustrated in the insets of panel (E), it is possible to cancel at the same time z-component of the visible (532nm) and x-component of the IR using a film thickness around 150nm on silver and an appropriate choice of angles of incidence, leaving only xxz contribution from $z_0 = 0$ interface. For the sapphire/PDMS/gold system, obviously a visible beam at 532nm is not appropriate, but at 800nm there is a nice crossing point between the SFG z-component and the IR x-component, with contrast ratios above 100:1 and 200:1, respectively, leaving again only xxz contribution.

4. Dielectric/metal/dielectric systems

In this last example, we turn to the system sapphire/metal/water described in Ref. 12. From the theoretical analysis, we know that no periodic minima are expected, still a non periodic configuration along case (i)-c is conceivable if the optical properties of the metal are close to those of a free electron gas. This means that no contrast due to Fresnel cancellation at $z_0 = 0$ may be expected for the y component this time. In order to reach contrast on *ssp*, *sps* and *pss* combinations, we therefore rely on z-component. As above, we check on Fig. 6 the existence of clear minima in the contrast factors $|R_x|^2$ and $|R_z|^2$ above the TIR critical angle (49°) of the sapphire/water system for silver (A) at 532nm (maximal contrast ratios 40000:1 for x and 850:1 for z) and (C) 800nm (80000:1 and 1100:1), and for gold (D) at 800nm (27000:1 and 300:1). For gold in the interband region (B), as in the previous case, minima become quickly useless when the thickness increases above 20 nm, leading to a very poorly defined transition from x to z as a function of increasing angle of incidence. Maximal

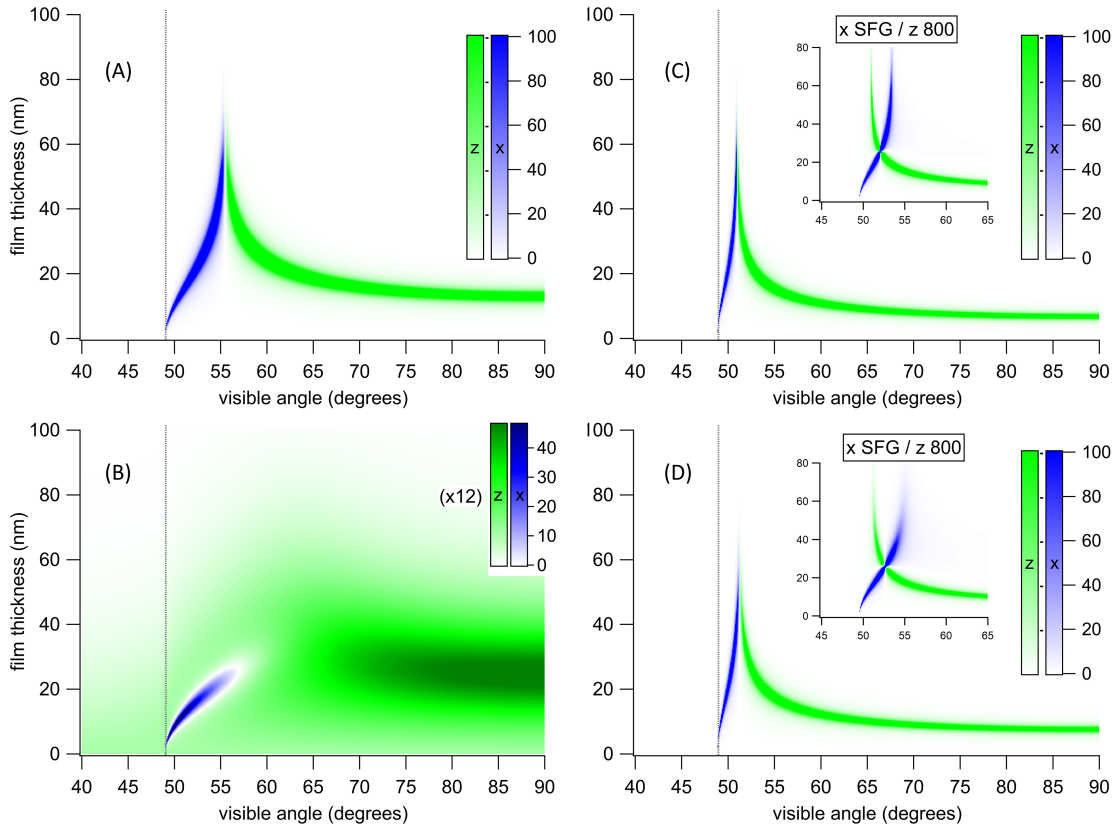

FIG. 6. Contrast factors in the visible at the sapphire/metal/water systems. 2D plot of $|1/R_x|^2$ (blue) and $|1/R_z|^2$ (green) for silver (A, C) and for gold (B, D) as a function of film thickness and visible angle of incidence in sapphire (z factors evaluated in medium [2]). Visible wavelengths are 532nm (A-B) and 800nm (C-D). Insets in panels (C) and (D) show the $|1/R_z|^2$ ratio at 800nm with $|1/R_x|^2$ at the SFG wavelength (IR wavenumber 3300cm^{-1}) for a visible at 800nm. Dotted lines indicate the critical angle for total internal reflection at the {sapphire/PDMS} interface. In panel (B), z contrast ratio is multiplied by 12.

contrast ratios reach 80:1 for $|R_x|^2$ close to the critical angle but drop down to 37:1 at 20nm thickness, whereas maximal $|R_z|^2$ does not exceed 4:1. In the infrared, the strong absorption of water completely damps the minima. An interesting crossing point may still be used in the *ppp* configuration with a visible wavelength set to 800nm, leading to an SFG wavelength still below the interband threshold. Minima for x and z are thus well defined, and a crossing point may be evidenced in the insets of panels (C) and (D) between x-component for SFG and z-component for the visible, leading to the selection of contribution zxx only at $z_0 = 0$ interface. Still, placing a molecular monolayer at this interface does not guarantee that its

zxx response may be experimentally measured, as the x Fresnel factor in the IR remains very unfavourable through $(1 - r_p^{12})$, with $r_p^{12} \approx 1$. As a conclusion, a Fresnel analysis of this system is relevant to analyze SFG signals produced by a molecular layer at the $z_0 = D$ interface,[12] but not much to increase the contrast between both interfaces.

The total SFG response also encompasses a bulk contribution from the metal layer [2]. If no other SFG source is present (e.g. no molecular monolayer is implemented in the system), then the complete response originates in the metal and is the sum of bulk and surface SFG from both interfaces. For very thin layers, the bulk contribution may be approximated by a surface one proportional to D.[90] In the general case, its dependence on D is more complicated but may be determined.[90] Combining these results on bulk with those elaborated above for a dielectric/metal/dielectric system, it is therefore conceivable to design experiments dedicated to experimentally separate and independently quantify surface and bulk metal contributions to SFG using smart choices of dielectric natures, metal thicknesses and angles of incidence.

VI. CONCLUSION

We have defined four configurations to desing three layer systems in which the SFG response of the first interface may be minimized or even canceled. The first one, composed of three dielectric materials, does not involve metal or highly absorbing material, but relies on total internal reflection configuration and is limited in a specific range of angles of incidence. In the second one, the last dielectric is replaced by a metal, creating a rather classical configuration for SFG. No TIR is needed, so the full range of incidence angles is accessible. The only limit lies in the screening of s-polarized contributions at the dielectric metal interface, especially in the infrared. Still this configuration is easy to handle and opens promising ways for fundamental studies at the dielectric/metal interface. Contrast enhancement in these two configurations have been addressed in particular cases in the past,[15,20,22] here we prove in addition their periodicity as a function of film thickness. The last two configurations are original, but more delicate to implement as they propose only one possibility to match thickness to angle of incidence. Still it should be possible to experimentally reach such high contrast configurations by careful adjustment of incidences, and monitor the predicted switch from x to z of the contrast cancellation in these systems. We hope that these predictions will motivate experimenters to check their accuracy on real systems in the

future.

With a broader perspective, these rules may be extended to interfaces comprising more than three layers. In particular, as will be shown in the next paper,[18] they act as the elementary building block of a scenario in which, in an N-layer system, high contrast is achieved not only between the last and next-to-last interfaces, but in general between the last interface and all the others. This will give access to an actual specificity of SFG spectroscopy of the most buried interface in realistic multilayer systems, an exciting perspective indeed.

Appendix A: Rules for high Fresnel contrast

1. General analysis

In this section, we look for the conditions leading to minimizing or cancelling the ratios $|R_{x/y/z}|$ in Eq. 65-67, i.e. favouring the response of the buried interface with respect to the first one. Both interfaces exchange their roles for the SFG beam when transmitted SFG is considered. When thickness D increases, the numerators (i.e. Fresnel factors at $z_0 = 0$: $1 - r_p^{23} e^{2i\beta_i}$ for x, $1 + r_s^{23} e^{2i\beta_i}$ for y and $1 + r_p^{23} e^{2i\beta_i}$ for z) vary in amplitude and phase. The denominators (i.e. factors at $z_0 = D$) vary essentially in phase for low absorbing materials, still their amplitudes integrate absorption $e^{-\mathbb{Im}(\beta_i)}$ when relevant while traveling through medium [2]. In order to keep contrast at an interesting level, one should consider keeping absorption to a low level in this medium, either choosing a low absorbing material or using small thicknesses. Consequently, changes in the amplitudes of the ratios mostly depend on the numerators (with one exception, detailed below for p-polarization and $|r_p^{23}| > 1$). We focus on one of the three beams (dropping indices i) and investigate the general case, defined by the following: (i) medium [1] is supposed to be a non absorptive dielectric where light propagates (i.e. no evanescent wave) leading to $n^{[1]}$ and $\theta^{[1]}$ real and positive. Other situations (e.g. absorptive medium [1]) may be adapted[91] as long as they verify $n^{[1]} \sin\theta^{[1]}$ real positive, or at least fulfill the conditions below on $\cos\theta^{[2]}$ and $n^{[2]} \cos\theta^{[2]}$; (ii) $n^{[2]}$, $n^{[3]}$, $\cos\theta^{[2]}$ and $\cos\theta^{[3]}$ take any allowed value in the complex plane, except 0. This makes possible to account for all situations in media [2] and [3]: absorptive dielectric, any metal, total internal reflection (TIR). From our notations, we have $\mathbb{Re}(n^{[2/3]})$ and $\mathbb{Im}(n^{[2/3]})$ positive (i.e. they belong to the upper right quarter of the complex

plane). From $\cos\theta^{[2]} = \sqrt{1 - \dfrac{(n^{[1]})^2 \sin^2\theta^{[1]}}{(n^{[2]})^2}}$ and $n^{[2]}\cos\theta^{[2]} = \sqrt{(n^{[2]})^2 - (n^{[1]})^2\sin^2\theta^{[1]}}$, it is straightforwardly checked that $\cos\theta^{[2]}$ and $n^{[2]}\cos\theta^{[2]}$ belong to the upper right quarter too, as do $\cos\theta^{[3]}$ and $n^{[3]}\cos\theta^{[3]}$. Finally, $\beta = \dfrac{\omega D}{c} n^{[2]}\cos\theta^{[2]} = \beta^R + i\beta^I$ verifies β^R and β^I positive.

2. *s*-polarization

Here we focus on minimizing or cancelling $|1 + r_s^{23}e^{2i\beta}| = |1 + r_s^{23}e^{-2\beta^I}e^{2i\beta^R}|$. Using $r_s^{23} = (p^{[2]} - p^{[3]})/(p^{[2]} + p^{[3]})$ with $p^{[i]} = n^{[i]}\cos\theta^{[i]}$ belonging to the upper right quarter of the complex plane, we see (Fig. 7B) that $|r_s^{23}| \leqslant 1$. For nonvanishing β^R and β^I, function $1 + r_s^{23}e^{2i\beta}$ follows a decreasing spiral for increasing values of D, from $1 + r_s^{23}$ to 1, whatever the phase of r_s^{23} (Fig. 7A). Rotation on the spiral is governed by $2\beta^R$, whereas the distance to 1 decreases as $e^{-2\beta^I}$ or, equivalently, the rotation rate is $\dfrac{2\omega}{c}\,\mathbb{R}\mathrm{e}(n^{[2]}\cos\theta^{[2]})$ and the attenuation rate $\dfrac{2\omega}{c}\,\mathbb{I}\mathrm{m}(n^{[2]}\cos\theta^{[2]})$ as a function of D. Consequently, there exists a series of minima of $|1 + r_s^{23}e^{2i\beta}|$ for the values of $D = D_s^M$ corresponding to points M_1, M_2, $\cdots$, where the spiral crosses the real axis, with a period equal to $\lambda/2\,\mathbb{R}\mathrm{e}(n^{[2]}\cos\theta^{[2]})$. At these points, $r_s^{23}e^{2i\beta^R}$ is real and negative and we have $|1 + r_s^{23}e^{2i\beta}| = 1 - |r_s^{23}|e^{-2\beta^I}$. As their distance from the origin grows when D increases, these minima are less and less marked: the bigger $\mathbb{I}\mathrm{m}(n^{[2]}\cos\theta^{[2]})/\,\mathbb{R}\mathrm{e}(n^{[2]}\cos\theta^{[2]})$, the stronger their damping. In addition, absorption driven by $\mathbb{I}\mathrm{m}(n^{[2]}\cos\theta^{[2]})$ also impacts R_y through the Fresnel factor at interface $z_0 = D$. When this phenomenon is taken into account, ratio $(1 + r_s^{23}e^{2i\beta})/e^{-\beta^I}$ (i.e. the full D-dependent amplitude of R_y) still follows a spiral as a function of D, which now converges towards a point e^{β^I} on the real axis, bigger than 1 and moving towards higher and higher values. This leads to an additional damping of the minima with growing D, but does not modify D_s^M values. Conversely, many minima will clearly show up with increasing D when attenuation $\dfrac{\omega}{c}\,\mathbb{I}\mathrm{m}(n^{[2]}\cos\theta^{[2]})$ is small as compared to rotation rate $\dfrac{\omega}{c}\,\mathbb{R}\mathrm{e}(n^{[2]}\cos\theta^{[2]})$. The values of D_s^M corresponding to the minima are found by solving $\mathbb{I}\mathrm{m}(r_s^{23}e^{2i\beta^R}) = 0$, leading to $\mathbb{I}\mathrm{m}(r_s^{23})\cos 2\beta^R + \mathbb{R}\mathrm{e}(r_s^{23})\sin 2\beta^R = 0$ or

$$\tan(2\beta^R) = \frac{2\ \mathbb{I}\mathrm{m}(\overline{n^{[3]}\cos\theta^{[3]}}\,n^{[2]}\cos\theta^{[2]})}{|n^{[3]}\cos\theta^{[3]}|^2 - |n^{[2]}\cos\theta^{[2]}|^2}, \tag{A1}$$

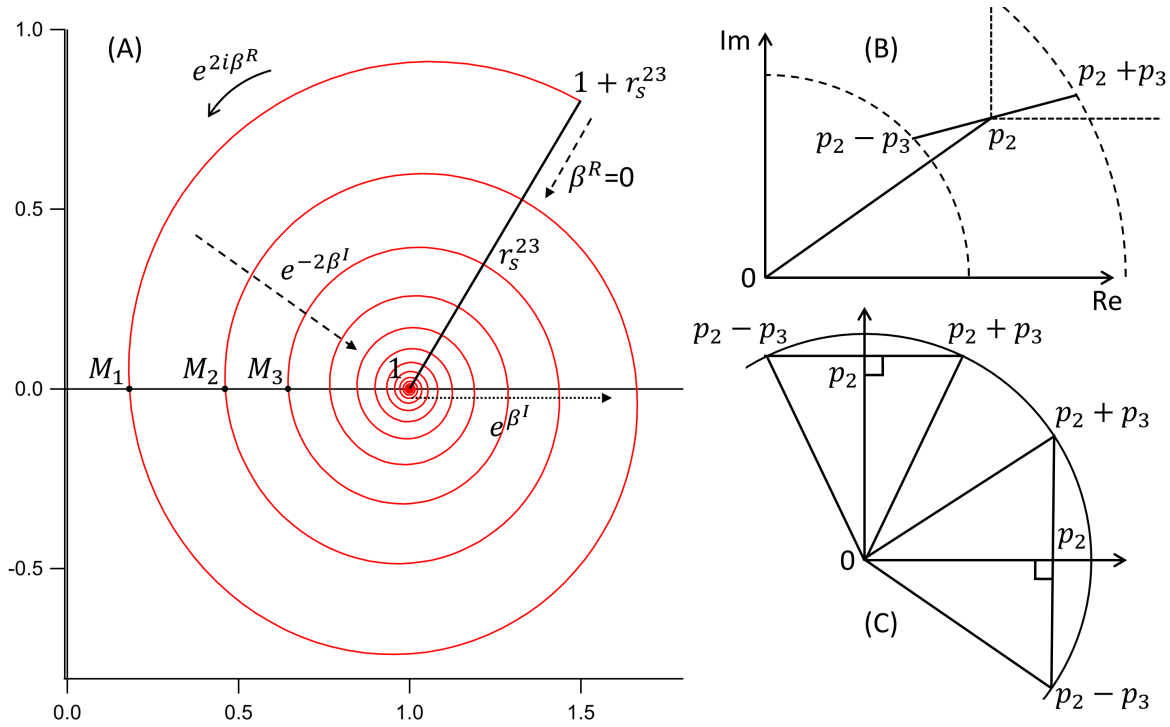

FIG. 7. (A) Evolution of $1 + r_s^{23} e^{2i\beta}$ as a function of increasing thickness D. Starting point for $D = 0$ is $1 + r_s^{23}$, with no constraint on the phase of r_s^{23}. Plain arrow show the rotation on the spiral ($e^{2i\beta^R}$), dashed arrows the decrease in amplitude ($e^{-2\beta^I}$). For contrast ratio R_y, convergence point of the spiral additionally moves along the dotted arrow. (B) Graphical illustration of $|r_s^{23}| \leqslant 1$. (C) The only possibilities for $|r_s^{23}| = 1$ with $p^{[2]}$ and $p^{[3]}$ belonging to the upper right quarter.

from which the values of D_s^M follow

$$D_s^M = \frac{\lambda}{4\pi\, \mathbb{R}\mathrm{e}(n^{[2]} \cos\theta^{[2]})} \left[\arctan\left(\frac{2\, \mathbb{I}\mathrm{m}(\overline{n^{[3]} \cos\theta^{[3]}}\, n^{[2]} \cos\theta^{[2]})}{|n^{[3]} \cos\theta^{[3]}|^2 - |n^{[2]} \cos\theta^{[2]}|^2} \right) + m\pi \right] \qquad \text{(A2)}$$

where $m = 2k$ when $|n^{[2]} \cos\theta^{[2]}| < |n^{[3]} \cos\theta^{[3]}|$ and $m = 2k + 1$ when $|n^{[2]} \cos\theta^{[2]}| > |n^{[3]} \cos\theta^{[3]}|$. When $\beta^R = 0$, there is no rotation in the complex plane anymore. The values of the Fresnel factors at $z_0 = 0$ vary with increasing D on a segment from $1 + r_s^{23}$ to 1: there is no minimum (Fig. 7A).

At points $\{M_i\}$, we have seen that the minima of $|1 + r_s^{23} e^{2i\beta}|$ take the value $1 - |r_s^{23}| e^{-2\beta^I}$. We see that, if $\beta^I = 0$ (i.e. no absorption in medium [2]), all minima have the same value $1 - |r_s^{23}|$: the spiral becomes a circle, which is indefinitely travelled when D grows, with a period equal to $\lambda / 2n^{[2]} \cos\theta^{[2]}$. In addition, absorption does not disturb this time the Fresnel factor at $z_0 = D$, and the contrast depends only on the value of $|r_s^{23}|$. Maximum contrast

(in favor of the SFG response at the $z_0 = D$ interface) is obtained when the Fresnel factor at $z_0 = 0$ vanishes, that is when $|r_s^{23}| = 1$ and $\beta^I = 0$. For the first condition, we have $|p^{[2]} - p^{[3]}| = |p^{[2]} + p^{[3]}|$. It is easily graphically seen that this implies that the phases of $p^{[2]}$ and $p^{[3]}$ differ by 90°, leading to only two possibilities (Fig. 7C). Adding the second condition, the only possibility left is $n^{[2]} \cos\theta^{[2]}$ real positive and $n^{[3]} \cos\theta^{[3]}$ imaginary positive, leading to the two cancellation solutions detailed in the main text: $\cos\theta^{[3]}$ imaginary (i.e. TIR propagation in dielectric medium [3], case (i)-a) or $n^{[3]}$ imaginary (i.e. case (ii)-a, e.g. free electron metal). Writing Eq. A1 as

$$\tan(2\beta) = \frac{2\ \mathbb{I}\mathrm{m}\left(\dfrac{n^{[2]}\cos\theta^{[2]}}{n^{[3]}\cos\theta^{[3]}}\right)}{1 - \left|\dfrac{n^{[2]}\cos\theta^{[2]}}{n^{[3]}\cos\theta^{[3]}}\right|^2}, \tag{A3}$$

with $n^{[3]}\cos\theta^{[3]} = i|n^{[3]}\cos\theta^{[3]}|$, we get

$$\tan(2\beta) = \frac{2\tan\beta}{1-\tan^2\beta} = \frac{2\,\dfrac{n^{[2]}\cos\theta^{[2]}}{in^{[3]}\cos\theta^{[3]}}}{1 - \left(\dfrac{n^{[2]}\cos\theta^{[2]}}{in^{[3]}\cos\theta^{[3]}}\right)^2}, \tag{A4}$$

leading to Eq. 66. This shows that there are no other possibilities to cancel the Fresnel factor at $z_0 = 0$ for s-polarization than those described in Part IV.

3. p-polarization

Minima for the Fresnel factors at $z_0 = 0$ are obtained when $|1 - r_p^{23} e^{2i\beta}|$ (for x component) and $|1 + r_p^{23} e^{2i\beta}|$ (for z component) are minimal. The great difference with the previous case lies in the expression of $r_p^{23} = (q^{[2]} - q^{[3]})/(q^{[2]} + q^{[3]})$ with $q^{[i]} = \cos\theta^{[i]}/n^{[i]}$. This time $q^{[i]}$ is only known to have a positive real part, which implies that $|r_p^{23}|$ is not bounded by 1. For nonvanishing β^R and β^I, the complex amplitudes at $z_0 = 0$ for x and z component follow two spirals symmetric with respect to 1, which this time may cross the imaginary axis (Fig. 8A) depending on the value of $|r_p^{23}|$. Minima in this case have a value analogous to s-polarization, i.e. $1 - |r_p^{23}| e^{-2\beta^I}$.

When $|r_p^{23}| \leqslant 1$, the analysis is identical to the s-polarisation case. Minima $\{M_i\}$ are all located on the right half of the complex plane (Fig. 8A), they show up for increasing D as long as β^I is not too big as compared to β^R. Their amplitudes decrease with increasing D,

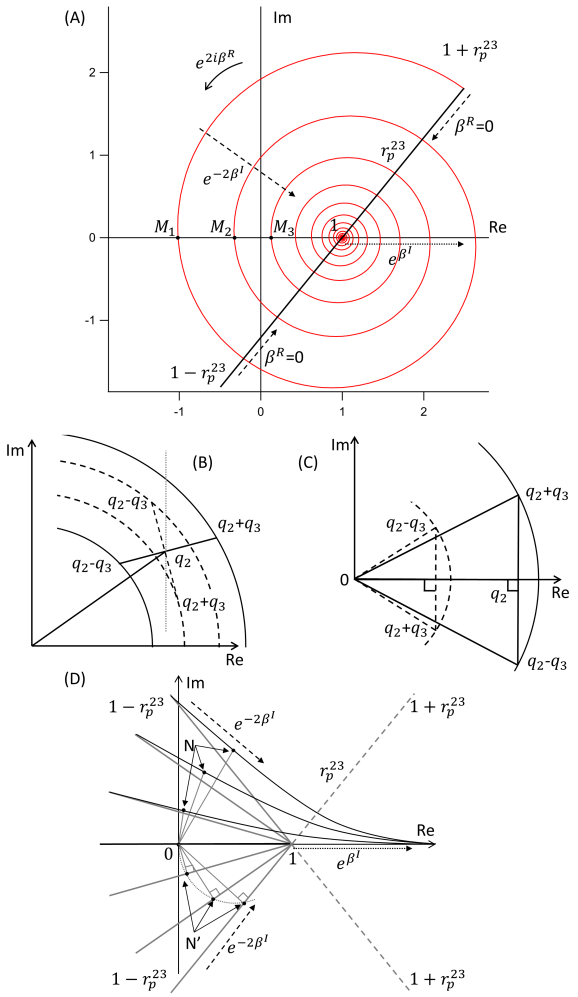

FIG. 8. (A) Evolution of $1 + r_p^{23} e^{2i\beta}$ as a function of increasing thickness D for $|r_p^{23}| > 1$. Starting point for $D = 0$ is $1 + r_p^{23}$, with no constraint on the phase of r_p^{23}. Number $1 - r_p^{23} e^{2i\beta}$ follows an analogous spiral, symmetric with respect to 1. Dashed arrows illustrate the decrease in amplitude $(e^{-2\beta^I})$. For contrast ratios R_x and R_z, convergence point of the spiral additionally moves along the dotted arrow. (B) Graphical illustration that $|r_p^{23}|$ may be smaller or bigger than 1. (C) The two possibilities leading to $|r_p^{23}| = 1$ with q_2 and q_3 having a positive real part. (D) Particular case $\beta_R = 0$ with $\mathbb{R}\mathrm{e}(1 - r_p^{23}) \leqslant 0$. Points N indicate minima for $|R_x|$, points N' minima for $1 - r_p^{23} e^{-2\beta_I}$.

except in the circle case for vanishing β^I, and they have the same period $\lambda/2\,\mathbb{R}\mathrm{e}(n^{[2]} \cos\theta^{[2]})$ as above. The symmetry between x and z spirals shows that their own minima correspond to $e^{2i\beta^R}$ out of phase by a half period, hence D_x^M and D_z^M differ by $\lambda/4\,\mathbb{R}\mathrm{e}(n^{[2]} \cos\theta^{[2]})$. Their

values follow from Eq. A1 by changing $p^{[i]}$ into $q^{[i]}$, leading to:

$$\tan(2\beta^R) = \frac{2\ \mathbb{I}\mathrm{m}(\overline{n^{[2]}\cos\theta^{[3]}}\, n^{[3]}\cos\theta^{[2]})}{|n^{[2]}\cos\theta^{[3]}|^2 - |n^{[3]}\cos\theta^{[2]}|^2}, \tag{A5}$$

and

$$D^M_{x/z} = \frac{\lambda}{4\pi\,\mathbb{R}\mathrm{e}(n^{[2]}\cos\theta^{[2]})}\left[\arctan\left(\frac{2\ \mathbb{I}\mathrm{m}(\overline{n^{[2]}\cos\theta^{[3]}}\, n^{[3]}\cos\theta^{[2]})}{|n^{[2]}\cos\theta^{[3]}|^2 - |n^{[3]}\cos\theta^{[2]}|^2}\right) + m\pi\right] \tag{A6}$$

This time, $m \geqslant 0$ takes all integer values, even m give D^M_x and odd m give D^M_z when $|n^{[3]}\cos\theta^{[2]}| > |n^{[2]}\cos\theta^{[3]}|$, and vice versa when $|n^{[3]}\cos\theta^{[2]}| < |n^{[2]}\cos\theta^{[3]}|$. Condition on D leading to exact cancellation at the minima is again obtained when $1 - |r_p^{23}|e^{-2\beta^I} = 0$, that is $\beta^I = 0$ and $|r_p^{23}| = 1$. With the first condition, we have $n^{[2]}\cos\theta^{[2]}$ real, implying both $n^{[2]}$ and $\cos\theta^{[2]}$ either real or imaginary positive. Only the first case being possible, we also have $\cos\theta^{[2]}/n^{[2]}$ real positive. The second condition translates as above into a 90° phase difference between q_2 and q_3, that is $\cos\theta^{[3]}/n^{[3]}$ is imaginary, either positive (i.e. $n^{[3]}$ real positive and $\cos\theta^{[3]}$ imaginary positive), and we recover case (i)-a; or negative (i.e. $n^{[3]}$ imaginary positive and $\cos\theta^{[3]}$ real positive), and we recover case (ii)-a. Again this shows here that there are no other possibilities for the cancellation of the Fresnel factors at $z_0 = 0$ when $|r_p^{23}| \leqslant 1$.

However, the case $|r_p^{23}| > 1$ still has to be investigated. In this case, for nonvanishing β^R and β^I, the first $\{M_i\}$ points are located on the left half of the complex plane (Fig. 8A). When D increases, they move towards the right half. This shows that the amplitudes at the minima first increase towards a highest value, close to the origin, then decrease as in the $|r_p^{23}| \leqslant 1$ case. Again, the rate of this two-step process as a function of D depends on ratio $\mathbb{I}\mathrm{m}(n^{[2]}\cos\theta^{[2]})/\,\mathbb{R}\mathrm{e}(n^{[2]}\cos\theta^{[2]})$. It is also further modulated in R_x and R_z by the absorption term in the $z_0 = D$ factor (e^{β^I}, as above), shifting the convergence point of the spiral to the right, and all minima further from the origin, increasing this way their damping. In this situation, there is in general no value for D leading to exact cancellation of the Fresnel factor at $z_0 = 0$, as the spiral does not cross the origin, except for a numerical coincidence. As was seen for s-polarization, when $\beta^I = 0$, the spiral becomes a circle and all minima have the same amplitude $1 - |r_p^{23}|$, which depends on the distance between $|r_p^{23}|$ and 1.

When $\beta^R = 0$ (i.e. $n^{[2]}\cos\theta^{[2]}$ is imaginary positive), whatever the value of $|r_p^{23}|$, the complex values vary as $e^{-2\beta^I}$ on a segment from $1 - r_p^{23}$ (x component) and $1 + r_p^{23}$ (z component) to 1 with increasing D. For $|r_p^{23}| \leqslant 1$, there is again no minimum. However,

when $|r_p^{23}| > 1$, one of the numbers $1 - r_p^{23}$ or $1 + r_p^{23}$ may have a negative real part (we explicitly treat here the case $1 - r_p^{23}$). When D increases, its modulus first decreases then increases, generating a new set of minima (N' points on Fig. 8D). They don't belong to a periodic series but are related to single D values. However, these minima are rather shallow as a function of D when β^I (i.e. $|n^{[2]} \cos\theta^{[2]}|$) is small, and when the segment passes far from the origin (e.g. $|\,\mathbb{I}\mathrm{m}(r_p^{23})| > |\,\mathbb{R}\mathrm{e}(1 - r_p^{23})|$). On the contrary, we expect a clear contrast when $|\,\mathbb{I}\mathrm{m}(r_p^{23})| \ll |\,\mathbb{R}\mathrm{e}(1 - r_p^{23})|$. However, in this situation the effect is completely due to β^I, so absorption at interface $z_0 = D$ must be taken into account in ratios $R_{x/z}$. As above, this implies that, as D increases, the end point of the previous "segments" also move from 1 to higher values e^{β^I}, and the segments transform into curves as sketched on Fig. 8D. Points N correspond to the minimal distances between these curves and the origin, and represent the true minima of contrast factors R_x and R_z. As the existence of such a minimum is due to the imaginary (i.e. absorptive) part of β, one may fear that absorption in medium [2] leads to a very small amount of light reaching interface $z_0 = D$, so that the minimum at point N corresponds to conditions where no signal is produced at $z_0 = D$. This cannot be the case because the minimum is reached through a modulation of r_p^{23} by $e^{-2\beta^I}$, which must thus have a finite (i.e. nonvanishing) value, implying in turn that absorption in medium [2] does not hamper SFG production at $z_0 = D$ interface. The corresponding values of D_x^N and D_z^N may be found by minimizing function $|1 \pm r_p^{23} e^{-2\beta^I}|/e^{-\beta^I} = |e^{\beta^I} \pm r_p^{23} e^{-\beta^I}|$, which by differentiation with respect to β^I leads to $|r_p^{23}| = e^{2\beta^I}$ and values

$$D_x^N = D_z^N = \frac{\lambda}{4\pi\,\mathbb{I}\mathrm{m}(n^{[2]}\cos\theta^{[2]})} \ln\left(|r_p^{23}|\right) \tag{A7}$$

For a comparison, the minima for the Fresnel factors at $z_0 = 0$ alone (points N') correspond to $\mathbb{R}\mathrm{e}(1/r_p^{23}) = e^{-2\beta^I}$ and

$$D_x^{N'} = D_z^{N'} = \frac{\lambda}{4\pi\,\mathbb{I}\mathrm{m}(n^{[2]}\cos\theta^{[2]})} \ln\left(\frac{|r_p^{23}|^2}{|\,\mathbb{R}\mathrm{e}(r_p^{23})|}\right) \tag{A8}$$

In particular, when $1 + r_p^{23}$ is a negative real number, point N (overlapping with point N') corresponds to the exact cancellation of the R_z contrast ratio, whereas cancellation for R_x occurs when $1 - r_p^{23}$ is a negative real number. As has been seen for s polarization, $n^{[2]}\cos\theta^{[2]}$ imaginary positive (i.e. $\beta^R = 0$) leads to two possibilities: $\cos\theta^{[2]}$ imaginary ($n^{[2]}$ real, i.e. TIR propagation in medium [2]) or $n^{[2]}$ imaginary ($\cos\theta^{[2]}$ real, e.g. free electron metal). In both situations, $q^{[2]}$ is also imaginary, respectively positive and negative.

As r_p^{23} must be a real number with $|r_p^{23}| > 1$, $q^{[3]}$ must also be imaginary, with its sign opposite to $q^{[2]}$. Summarizing all points above, cancellation is obtained when $\cos\theta^{[2]}$ and $n^{[3]}$ are imaginary [case (ii)-b], or when $n^{[2]}$ and $\cos\theta^{[3]}$ are imaginary [case (i)-c]. The sign of real number r_p^{23} therefore depends on the sign of $q^{[2]} + q^{[3]}$ on the imaginary axis. When $|q^{[2]}| > |q^{[3]}|$, r_p^{23} is positive and only R_x may vanish, whereas for $|q^{[2]}| < |q^{[3]}|$ only R_z may vanish. Cancellation for x or z therefore depends whether ratio $\left|\dfrac{n^{[3]}\cos\theta^{[2]}}{n^{[2]}\cos\theta^{[3]}}\right|$ is bigger (for x) or smaller (for z) than 1. The corresponding values of D follow from $|r_p^{23}| = e^{2\beta^I}$, which is solved, using $|q^{[2]} - q^{[3]}| = |q^{[2]}| + |q^{[3]}|$ and $|q^{[2]} + q^{[3]}| = \mathrm{abs}(|q^{[2]}| - |q^{[3]}|)$ in this particular case, into $\tanh(\beta^I) = |q^{[3]}|/|q^{[2]}|$ for x-component, and $\tanh(\beta^I) = |q^{[2]}|/|q^{[3]}|$ for z-component, with $\beta^I = \dfrac{2\pi D\,\mathbb{I}\mathrm{m}(n^{[2]}\cos\theta^{[2]})}{\lambda}$, recovering the results of (i)-c (Eq. 74) and (ii)-b (Eq. 78) in Part IV. Exact cancelling at the minimum requires that $q^{[2]}$ or $q^{[3]}$ is imaginary positive (TIR) while the other is imaginary negative (imaginary index, i.e. metal). For other situations, minima may be obtained, instead of zeroes, when both media have properties close to the ideal ones above, that is one strongly absorbing ($\mathbb{I}\mathrm{m}(n^{[i]}) > \mathbb{R}\mathrm{e}(n^{[i]})$ (metal-like), and for the other $\mathbb{R}\mathrm{e}(n^{[i]}) > \mathbb{I}\mathrm{m}(n^{[i]})$ as long as $|n^{[1]}\sin\theta^{[1]}/n^{[i]}| > 1$ (TIR-like).

This full analysis in the complex plane shows that there is no other possibility to exactly cancel the contrast ratios R_x, R_y, R_z than those listed in Part IV. Gathering the results, we see that cancellation occurs when $|r_{s/p}^{23}| = 1$ and $\mathbb{I}\mathrm{m}(n^{[2]}\cos\theta^{[2]}) = 0$, or for r_p^{23} real with $|r_p^{23}| > 1$ and $\mathbb{R}\mathrm{e}(n^{[2]}\cos\theta^{[2]}) = 0$. By extension, the existence of a series of periodic minima with a high contrast is linked to the conditions that absorption $\dfrac{\omega}{c}\,\mathbb{I}\mathrm{m}(n^{[2]}\cos\theta^{[2]})$ is small as compared to rotation rate $\dfrac{\omega}{c}\,\mathbb{R}\mathrm{e}(n^{[2]}\cos\theta^{[2]})$, and that $|r_{s/p}^{23}|$ is close to 1. Additional (single) non-periodic minima are possible for p polarization when r_p^{23} is close to real and $|r_p^{23}| > 1$, provided that $\dfrac{\omega}{c}\,\mathbb{R}\mathrm{e}(n^{[2]}\cos\theta^{[2]})$ is small as compared to $\dfrac{\omega}{c}\,\mathbb{I}\mathrm{m}(n^{[2]}\cos\theta^{[2]})$.

SUPPLEMENTARY MATERIAL

See Supplementary Material for details on the origins of Fresnel dispersion in the infrared range.

DATA AVAILABILITY

The data that support the findings of this study are available from the corresponding author upon reasonable request.

REFERENCES

[1]X. Li and G. Rupprechter, Catal. Sci. Technol. **11**, 12 (2021).

[2]R. De and B. Dietzek-Ivanšić, Chem. Eur. J. **28**, e202200407 (2022).

[3]S. M. Piontek and E. Borguet, J. Phys. Chem. C **126**, 2307 (2022).

[4]F. M. Geiger and G. V. Hartland, J. Phys. Chem. B **126**, 6367 (2022).

[5]A. G. Lambert, D. J. Neivandt, A. M. Briggs, E. W. Usadi, and P. B. Davies, J. Phys. Chem. B **106**, 5461 (2002).

[6]H. Ye, A. Abu-Akeel, J. Huang, H. E. Katz, and D. H. Gracias, J. Am. Chem. Soc. **128**, 6528 (2006).

[7]P. M. Kearns, D. B. O'Brien, and A. M. Massari, J. Phys. Chem. Lett. **7**, 62 (2016).

[8]N. Bloembergen and P. S. Pershan, Phys. Rev. **128**, 606 (1962).

[9]J. E. Sipe, J. Opt. Soc. Am. B **4**, 481 (1987).

[10]T. F. Heinz, in *Nonlinear Surf. Electromagn. Phenom.*, edited by H. E. Ponath and G. I. Stegeman (Elsevier, Amsterdam, 1991) Chap. 5, pp. 353–416.

[11]S. J. McGall, P. B. Davies, and D. J. Neivandt, J. Phys. Chem. B **108**, 16030 (2004).

[12]E. H. G. Backus, N. Garcia-Araez, M. Bonn, and H. J. Bakker, J. Phys. Chem. C **116**, 23351 (2012).

[13]L. Wang, S. Nihonyanagi, K.-I. Inoue, K. Nishikawa, A. Morita, S. Ye, and T. Tahara, J. Phys. Chem. C **123**, 15665 (2019).

[14]M. B. Feller, W. Chen, and Y. R. Shen, Phys. Rev. A **43**, 6778 (1991).

[15]M. S. Azam, C. Cai, and D. K. Hore, J. Phys. Chem. C **123**, 23535 (2019).

[16]D. S. Bethune, J. Opt. Soc. Am. B **6**, 910 (1989).

[17]D. B. O'Brien and A. M. Massari, J. Opt. Soc. Am. B **30**, 1503 (2013).

[18]B. Busson, submitted to J. Chem. Phys. (2023).

[19]C. Hirose, H. Ishida, K. Iwatsu, N. Watanabe, J. Kubota, A. Wada, and K. Domen, J. Chem. Phys. **108**, 5948 (1998).

[20]X. Lu, N. Shephard, J. Han, G. Xue, and Z. Chen, Macromolecules **41**, 8770 (2008).

[21]X. Lu, D. Li, C. B. Kristalyn, J. Han, N. Shephard, S. Rhodes, G. Xue, and Z. Chen, Macromolecules **42**, 9052 (2009).

[22]C. Cai, M. S. Azam, and D. K. Hore, J. Phys. Chem. C **125**, 12382 (2021).

[23]D. E. Cotton and S. T. Roberts, J. Chem. Phys. **154**, 114704 (2021).

[24]E. G. Moloney, M. S. Azam, C. Cai, and D. K. Hore, Biointerphases **17**, 051202 (2022).

[25]J. J. Maki, M. Kauranen, and A. Persoons, Phys. Rev. B **51**, 1425 (1995).

[26]X. Zhuang, P. B. Miranda, D. Kim, and Y. R. Shen, Phys. Rev. B **59**, 12632 (1999).

[27]W. N. Hansen, J. Opt. Soc. Am. **58**, 380 (1968).

[28]G. Gonella, C. Lütgebaucks, A. G. F. de Beer, and S. Roke, J. Phys. Chem. C **120**, 9165 (2016).

[29]Y.-C. Wen, S. Zha, X. Liu, S. Yang, P. Guo, G. Shi, H. Fang, Y. R. Shen, and C. Tian, Phys. Rev. Lett. **116**, 016101 (2016).

[30]C. Hirose, N. Akamatsu, and K. Domen, Appl. Spectrosc. **46**, 1051 (1992).

[31]S. S. Andrews, J. Chem. Educ. **81**, 877 (2004).

[32]S. Roy, K.-K. Hung, U. Stege, and D. K. Hore, Appl. Spectrosc. Rev. **49**, 233 (2014).

[33]Y. Tong, Y. Zhao, N. Li, M. Osawa, P. B. Davies, and S. Ye, J. Chem. Phys. **133**, 034704 (2010).

[34]J. D. McIntyre and D. E. Aspnes, Surf. Sci. **24**, 417 (1971).

[35]X. Lu, M. L. Clarke, D. Li, X. Wang, G. Xue, and Z. Chen, J. Phys. Chem. C **115**, 13759 (2011).

[36]V. N. D. Piano and A. F. Quesada, Appl. Opt. **4**, 1386 (1965).

[37]E. D. Palik, H. Boukari, and R. W. Gammon, Appl. Opt. **35**, 38 (1996).

[38]J. Jerphagnon and S. K. Kurtz, J. Appl. Phys. **41**, 1667 (1970).

[39]X. Wei, P. B. Miranda, C. Zhang, and Y. R. Shen, Phys. Rev. B **66**, 085401 (2002).

[40]C.-C. Yu, T. Seki, K.-Y. Chiang, F. Tang, S. Sun, M. Bonn, and Y. Nagata, J. Phys. Chem. B **126**, 6113 (2022).

[41]B. Busson and L. Dalstein, J. Chem. Phys. **149**, 154701 (2018).

[42]C. Matranga and P. Guyot-Sionnest, J. Chem. Phys. **115**, 9503 (2001).

[43]D. Krause, C. W. Teplin, and C. T. Rogers, J. Appl. Phys. **96**, 3626 (2004).

[44]F. X. Wang, F. J. Rodríguez, W. M. Albers, R. Ahorinta, J. E. Sipe, and M. Kauranen, Phys. Rev. B **80**, 233402 (2009).

[45]B. S. Mendoza, W. L. Mochán, and J. A. Maytorena, Phys. Rev. B **60**, 14334 (1999).

[46]L. Dalstein, A. Revel, C. Humbert, and B. Busson, J. Chem. Phys. **148**, 134701 (2018).

[47]B. Busson and L. Dalstein, J. Chem. Phys. **149**, 034701 (2018).

[48]V. Mizrahi and J. E. Sipe, J. Opt. Soc. Am. B-Optical Phys. **5**, 660 (1988).

[49]E. K. L. Wong and G. L. Richmond, J. Chem. Phys. **99**, 5500 (1993).

[50]J. A. Maytorena, B. S. Mendoza, and W. L. Mochán, Phys. Rev. B **57**, 2569 (1998).

[51]A. G. Lambert, P. B. Davies, and D. J. Neivandt, Appl. Spec. Rev. **40**, 103 (2005).

[52]P. Guyot-Sionnest, J. H. Hunt, and Y. R. Shen, Phys. Rev. Lett. **59**, 1597 (1987).

[53]H. Wu, W. K. Zhang, W. Gan, Z. F. Cui, and H. F. Wang, J. Chem. Phys. **125**, 133203 (2006).

[54]K. C. Jena, K. K. Hung, T. R. Schwantje, and D. K. Hore, J. Chem. Phys. **135**, 044704 (2011).

[55]J. F. D. Liljeblad and E. Tyrode, J. Phys. Chem. C **116**, 22893 (2012).

[56]M. Born and E. Wolf, eds., *Principles of Optics*, 7th ed. (Cambridge University Press, 1999).

[57]H. Fearn, D. F. V. James, and P. W. Milonni, Am. J. Phys. **64**, 986 (1996).

[58]D.-S. Zheng, Y. Wang, A.-A. Liu, and H.-F. Wang, Int. Rev. Phys. Chem. **27**, 629 (2008).

[59]Y. R. Shen, J. Chem. Phys. **153**, 180901 (2020).

[60]R. P. Feynman, R. B. Leighton, and M. Sands, eds., *The Feynman lectures on Physics*, millenium edition ed., Vol. 1 (Basic Books, 2011).

[61]Y. R. Shen, Annu. Rev. Phys. Chem. **40**, 327 (1989).

[62]W. Gan, D. Wu, Z. Zhang, R.-r. Feng, and H.-F. Wang, J. Chem. Phys. **124**, 114705 (2006).

[63]W.-C. Yang, B. Busson, and D. K. Hore, J. Chem. Phys. **152**, 084708 (2020).

[64]J. Wang, M. L. Clarke, and Z. Chen, Analytical Chem. **76**, 2159 (2004).

[65]B. Busson and L. Dalstein, J. Phys. Chem. C **123**, 26597 (2019).

[66]L. Dalstein, C. Humbert, M. Ben Haddada, S. Boujday, G. Barbillon, and B. Busson, J. Phys. Chem. Lett. **10**, 7706 (2019).

[67]Y. He, H. Ren, E.-M. You, P. M. Radjenovic, S.-G. Sun, Z.-Q. Tian, J.-F. Li, and Z. Wang, Phys. Rev. Lett. **125**, 047401 (2020).

[68]B. Humbert, J. Grausem, A. Burneau, M. Spajer, and A. Tadjeddine, Appl. Phys. Lett. **78**, 135 (2001).

[69]A. Bouhelier, M. Beversluis, A. Hartschuh, and L. Novotny, Phys. Rev. Lett. **90**, 013903 (2003).

[70]Y. Shen, J. Swiatkiewicz, J. Winiarz, P. Markowicz, and P. N. Prasad, Appl. Phys. Lett. **77**, 2946 (2000).

[71]R. D. Schaller, J. C. Johnson, K. R. Wilson, L. F. Lee, L. H. Haber, and R. J. Saykally, J. Phys. Chem. B **16**, 5143 (2002).

[72]T. A. Ishibashi and H. Onishi, Appl. Phys. Lett. **81**, 1338 (2002).

[73]C. Humbert, B. Busson, C. Six, A. Gayral, M. Gruselle, F. Villain, and A. Tadjeddine, J. Electroanal. Chem. **621**, 314 (2008).

[74]S. Yamaguchi, A. Kundu, P. Sen, and T. Tahara, J. Chem. Phys. **137** (2012), 10.1063/1.4758805.

[75]C. Humbert, Y. Caudano, L. Dreesen, Y. Sartenaer, A. Mani, C. Silien, J.-J. Lemaire, P. Thiry, and A. Peremans, Appl. Surf. Sci. **237**, 462 (2004).

[76]Q. Li, R. Hua, and K. C. Chou, J. Phys. Chem. B **112**, 2315 (2008).

[77]T. Miyamae, Y. Miyata, and H. Kataura, J. Phys. Chem. C **113**, 15314 (2009).

[78]T. Miyamae, K. Tsukagoshi, and W. Mizutani, Phys. Chem. Chem. Phys. **12**, 14666 (2010).

[79]T. Miyamae, E. Ito, Y. Noguchi, and H. Ishii, J. Phys. Chem. C **115**, 9551 (2011).

[80]D. Elsenbeck, S. K. Das, and L. Velarde, Phys. Chem. Chem. Phys. **19**, 18519 (2017).

[81]T. Noblet, L. Dreesen, S. Boujday, C. Méthivier, B. Busson, A. Tadjeddine, and C. Humbert, Commun. Chem. **1**, 76 (2018).

[82]W.-T. Liu and Y. R. Shen, Proc. Natl. Acad. Sci. U. S. A. **111**, 1293 (2014).

[83]S. A. R. Horsley and M. Woolley, Nat. Phys. **17**, 348 (2021).

[84]G. Li, A. Dhinojwala, and M. S. Yeganeh, J. Phys. Chem. C **115**, 7554 (2011).

[85]K. S. Gautam, A. D. Schwab, A. Dhinojwala, D. Zhang, S. M. Dougal, and M. S. Yeganeh, Phys. Rev. Lett. **85**, 3854 (2000).

[86]G. P. Harp, K. S. Gautam, and A. Dhinojwala, J. Am. Chem. Soc. **124**, 7908 (2002).

[87]R. Lu, W. Gan, B. H. Wu, Z. Zhang, Y. Guo, and H. F. Wang, J. Phys. Chem. B **109**, 14118 (2005).

[88]R. L. Olmon, B. Slovick, T. W. Johnson, D. Shelton, S. H. Oh, G. D. Boreman, and M. B. Raschke, Phys. Rev. B **86**, 235147 (2012).

[89]H. H. U. Yang, J. D'Archangel, M. L. Sundheimer, E. Tucker, G. D. Boreman, and M. B. Raschke, Phys. Rev. B **91**, 235137 (2015).

[90]B. Busson, submitted to J. Chem. Phys. (2023).

[91]J. Stratton, *Electromagnetic theory* (McGraw-Hill, New York, USA, 1941).